Assessment of infection probability indices for airborne diseases in confined spaces: combination of CFD and analytical modelling

Marzio Piller, Gabriele Bulian and Carlo Antonio Stival

Department of Engineering and Architecture, University of Trieste, Trieste, Italy

ABSTRACT

The paper presents a framework for probabilistic assessment of likelihood of infection from airborne diseases in confined spaces which are continuously occupied for relatively long periods (e.g., school classrooms). The proposed approach is based on a combination of computational fluid dynamics (CFD) pre-calculations and analytical post-processing, to define relevant indices of infection probability. The practical applicability of the method is demonstrated through a case study, where different ventilation scenarios are considered for a school classroom. Corresponding infection probability indices are determined globally for the group of occupants. Furthermore, since the method does not rely on the well-mixing assumption, local probability indices are determined for each occupied location. The obtained results confirm the intuition that an increase of ventilation and/or air filtration reduces the overall likelihood of infection, though the observed positive effect is not uniform within the space. The presented methodology can also be considered as complementary to simpler approaches.

1. Introduction

The coronavirus pandemic which started in 2019 has emphasized the relation between the airborne dispersion of droplets exhaled by an infected person and the spread of respiratory infections (Morawska and Cao 2020; Liu et al. 2008). It is known that SARS-CoV-2 remains viable and suspended in aerosols for several hours, having a half-life of the order of 1.1 hours (Morawska and Milton 2020; Prather, Wang, and Schooley 2020; van Doremalen et al. 2020; Wang et al. 2021), whereas the contact with fomites, such as workplace surfaces, represent a less likely transmission mode (Kampf et al. 2020; Meyerowitz et al. 2021). In this context, public buildings and, more generally, structures accessible to public represent a potentially critical situation, particularly in case of long-lasting presence of groups of occupants (e.g., school and university buildings, retail buildings, restaurants, concert halls, health-care settings, passenger ships, conference rooms, offices, auditoriums, sport centres, etc.) (Atkinson et al. 2009; Blocken et al. 2021; Cirrincione et al. 2020; Hu et al. 2022; Li and Tang 2022; Mizumoto and Chowell 2020; Ronchi and Lovreglio 2020; Bruinen de Bruin et al. 2020; Prem et al. 2020; Schade et al. 2021; Sharma, Bahga, and Gupta 2023; Szałański, Cepiński, and Sayegh 2023).

Aerosols, defined as small droplets or particles sizing at most 5 µm, can be associated with a higher infection risk than larger particles, because aerosols can remain suspended in air for long time periods and disperse over wide areas (Asadi et al. 2020; Cole and Cook 1998; Rencken et al. 2021; Sonkin 1951). The probability of transmitting an airborne infection in confined spaces is considered strongly dependent on airflow characteristic, ventilation parameters, geometry and distribution of people location in the space itself (Wang et al. 2022). Building factors and ventilation strategies play a central role in the removal of airborne infectious agents and have a consequent effect on the infection probability in confined spaces (Atkinson et al. 2009; Escombe et al. 2007; Schade et al. 2021). The effectiveness of ventilation systems is considered crucial for the containment of the infection probability in confined spaces (Atkinson et al. 2009; Cole and Cook 1998; Dai and Zhao 2020; Morawska et al. 2020; Szałański, Cepiński, and Sayegh 2023). For instance, Liu et al. (2008) investigate by numerical simulation the transmission of aerosol particles containing SARS virus between vertically-adjacent flats in a high-rise building. Their results show that, under favourable environmental conditions and with one-sided ventilation (one

window open, door closed), the buoyancy forces originating from the indoor-outdoor temperature difference induce a stream of contaminated air from the lower flat to the upper adjacent flat. The aforementioned transmission route was associated with the onset of small-scale SARS clusters occurred in several high-rise residential buildings in Hong Kong during the SARS epidemic in 2003 (Liu et al. 2008). Hu et al. (2022) analyse the SARS-CoV-2-infection risk and building energy consumption for different types of indoor spaces (shopping centres, restaurants, gyms, subway, railway station and others) using an improved Wells-Riley model accounting for dynamic quanta generation and pulmonary ventilation rate and a building energy consumption model based on the concept of equivalent fresh air volume. The study shows that significant energy savings could be attained by optimizing the rate of mechanical ventilation in terms of reducing the energy consumption while at the same time maintaining adequate prevention and control on the spreading of the SARS-CoV-2 infection. Szałański, Cepiński, and Sayegh (2023) assess the effect of leakages in in the heat recovery system of air-handling units on SARS-CoV-2 infection probability by exploiting the Wells-Riley model (Riley, Murphy, and Riley 1978; Riley 2001), for different types of indoor spaces.

Simulation tools have already been used to assess the effectiveness of mitigation measures against airborne virus diffusion, also in crowded situations (Abbas and Gursel Dino 2022; Fang et al. 2020; Gao, Niu, and Morawska 2008; Gao et al. 2016; Huang et al. 2022; Mirzaie et al. 2021; Mizumoto and Chowell 2020; Saari et al. 2006; Sharma, Bahga, and Gupta 2023). Lu et al. (1996) provide one of the first studies where Computational Fluid Dynamics (CFD) is used to predict the dispersion of aerosol particles in a ventilated indoor environment. A standard k-ε turbulence model is used to simulate the airflow, while a Lagrangian particle-tracking approach allows modelling the dispersion of aerosol particles. The Lagrangian approach allows predicting the dispersion of respiratory droplets, tracking their movement through space, thereof attempting to evaluate the associated infection probability (Peng, Chen, and Liu 2020; Vuorinen et al. 2020; Wang et al. 2022). Chung and Dunn-Rankin (1998) simulate the turbulent airflow distribution and the particle dispersion inside a small-scale model room under forced ventilation to assess the overall air ventilation efficiency in indoor spaces. For turbulent flow simulation they exploit a k-ε model, and particle dispersion is simulated using a Lagrangian approach. The numerical results are successfully validated by comparison against experimental measurements. Zhao et al. (2004) numerically investigate the efficiency of mixing and displacement ventilation for a model room, in terms of effectiveness in removing airborne aerosol particles of different diameters. The turbulent airflow within the room is modelled by the RNG – k-ε approach, which is widely adopted for indoor airflow simulations (Chen 1995). The study by Zhao et al. (2004) shows that aerosol particles in the considered diameter range of 1–10 μm are significantly affected only by the drag force, by the buoyancy force, by the Brownian force and by the shear-lift force (Li and Ahmadi 1992). According to Chen, Yu, and Lai (2006), the RNG – k-ε model is more suitable for indoor airflow simulation, and better agreement between simulated results and measured data has been achieved, compared to the standard k-ε and other turbulence or laminar models (Chen 1995; Posner, Buchanan, and Dunn-Rankin 2003). A different contaminant dispersion model is used by Abbas and Gursel Dino (2022) to predict the dispersion of infectious aerosol within a classroom. In particular, a CFD solver coupled with a zero-equation turbulence model provides the airflow distribution to an Eulerian model, which in turn returns the concentration of the contaminant throughout the computational domain. Wang and Chow (2015) use both a Lagrangian model and an Eulerian (drift-flux) model to simulate the dispersion of infectious airborne particles in a hospital environment, accounting for the presence and for the movements of the occupants. Sharma, Bahga, and Gupta (2023) simulate the airflow field and the dispersion of SARS-Cov-2 infected aerosol throughout two mechanically-ventilated university lecture rooms. The virus particles are modelled as a passive scalar (Eulerian approach) and resulting data are coupled with the Wells-Riley infection model (Riley, Murphy, and Riley 1978; Riley 2001).

Regarding the probabilistic modelling for the assessment of infection probabilities in confined spaces, taking into account also the statistical variation of sources of infection in the room, Iddon et al. (2022) recently presented an approach aiming at the quantification of the proportion of population newly infected. The approach by Iddon et al. (2022) relies on the well-mixing assumption and on the assumption of common properties for all the occupants in the considered space.

According to the current state of the art, it can be noticed that, on the one side, CFD has been used to simulate the details of dispersion of aerosols, and, on the other side, probabilistic approaches have been devised on the basis of simplified models for the underlying flow field and particle dispersion characteristics.

In this context, the present paper aims at making some steps forward, by presenting a framework for the probabilistic assessment of the likelihood of infection in confined spaces that are continuously occupied for relatively long periods. The approach is based on

the combination of CFD pre-calculations and analytical post-processing, to define relevant indices of infection probability. The use of CFD calculations aims at making a step forward with respect to the use of well-mixing assumption, and it allows having local information within the considered space. Then, the probabilistic post-processing presented in this study allows taking into account different relevant characteristic properties for the occupants, and, thanks to the combination with CFD pre-calculations, it provides specific information for occupants in different positions within the considered space.

The proposed framework is demonstrated via a case study, where different ventilation scenarios for a school classroom are compared on the basis of the calculated infection probability indices. Schools and classrooms have already been considered a challenge for strategies aiming to reduce the concentration of airborne infectious aerosol in spaces characterized by dense and long-lasting occupancy (Mirzaie et al. 2021; Abbas and Gursel Dino 2022) in view of the possible occurrence of overcrowding (Bartolucci, Templeton, and Bernardini 2022; D'angelo et al. 2021; D'Orazio, Bernardini, and Quagliarini 2021; Haug et al. 2020). For the specific case study presented in the paper, the simple Wells-Riley infection model is used (Riley, Murphy, and Riley 1978; Riley 2001), targeting the case of possible infections due to SARS-CoV-2. However, the approach presented herein is based on an unsteady local application of the Wells-Riley model, which is made possible by leveraging on the capabilities given by the coupling with CFD-based particle tracking simulations. From a modelling perspective, this allows making a step forward with respect to some shortcomings that have been highlighted in relation to the common use of the Wells-Riley model under well-mixing assumption (Noakes et al. 2006).

The paper is organised as follows. Section 2 describes the developed framework for the evaluation of infection probability indices in confined spaces. The section describes how CFD pre-calculations are used to provide relevant input data for the subsequent analytical post-processing, and it also provides details on the developed infection probability indices. Section 3 presents the aforementioned case study. Background information and calculation results are presented and discussed. The presented results show how to derive global and local infection probability indices, allowing for the classification of different occupied positions in terms of likelihood of infection. Furthermore, different ventilation scenarios are ranked according to the likelihood of spreading the infection through the occupants. Finally, section 4 provides the concluding remarks.

2. Methodology for the determination of infection probability indices

2.1. Overview

The proposed assessment methodology is based on a combination of CFD pre-calculations and a subsequent analytical post-processing of the obtained data, to define relevant infection probability indices for given scenarios. The wording "probability indices" is used herein rather than using the wording "probabilities" only to reflect the fact that final probability estimations from the proposed approach, and actually also from any other similar approach, are inevitably affected by the assumptions and simplifications embedded in the modelling.

In extreme summary, the developed approach can be outlined as follows:

(1) Given a ventilation scenario and relevant boundary conditions, CFD pre-calculations are carried out for the considered scenario. The scope of this step is to obtain the background flow field that is used for the subsequent analysis in step (2);
(2) Simulations of particle dispersions are performed considering exhalation from each occupant, using the background field determined in (1) as forcing field. The scope of this step is to determine how saliva droplets exhaled from each given occupant disperse in the room and eventually arrive at the other occupants of the room;
(3) The viral dose inhaled by each occupant is quantified by post-processing the results obtained from step (2);
(4) Probabilistic indices of infection are calculated on the basis of the results from step (3) by exploiting an infection model and by considering all possible cases of initially infected/not infected occupants in the room.

The approach aims to reduce the bottleneck due to the computational time which is typical of direct case-by-case application of CFD simulations. More details regarding the main steps are reported in the following and in the relevant sub-sections.

The key input for the determination of infection probability indices through the analytical probabilistic model described in section 2.3 is represented by the so-called viral dose inhaled by the generic susceptible occupant within a given exposure time. The virus is transported by saliva droplets exhaled by the infectious occupants in the occupied space. The probabilistic model takes into account the distribution of susceptible and infectious occupants in the given confined space, according to the probability that each available location is occupied by

an infectious occupant at the beginning of the exposure time. Calculations based on the probabilistic model are relatively simple and quick to be applied, once the inhaled viral dose is quantified.

To quantify the viral dose inhaled by a susceptible occupant within a given exposure time, resort is made to CFD pre-computations of particle dispersions (see section 2.4) combined with some reasonable simplifying assumptions. The concentration of the saliva droplets exhaled by each generic occupant is calculated in front of the other occupants, at each time instant. One major assumption is that the dispersion of saliva droplets does not influence the background flow field (so-called 1-way coupling regime). Furthermore, it is assumed that the volume concentration of the exhaled saliva droplets is sufficiently low to prevent their mutual interaction. As for the first assumption, the distinction between the 1-way or 2-way coupling regimes was addressed by Elghobashi (1994). The distinction between the two regimes depends on the particle loading and on the dimensionless particle Stokes number $St_p \equiv \tau_p/\tau_K$, where τ_p is the particle relaxation time (see, e.g., Kuerten (2016)) and τ_K is the Kolmogorov time scale (see, e.g., Pope (2000)). In the scenarios considered in the present work, the maximum volume fraction of saliva droplets occurs during exhalation, just in front of the mouth of the room's occupants where, based on the data reported in Table 2 for the considered case study (see section 3), the volume fraction is $\sim 1.38 \cdot 10^{-12}$ m^3 saliva / m^3 air. According to the results of Elghobashi (1994), for a volume fraction lower than $\sim 10^{-6}$ the flow-particle interaction is essentially 1-way, irrespective of the value of the particle Stokes number (see, e.g., Figure 1 in Kuerten (2016)). Regarding the second assumption, the particle-particle interaction becomes relevant only for even larger values of the particle loading (Kuerten 2016). In view of the above, the present flow-particle interaction can be considered as 1-way and the particle-particle interaction can be neglected. These two assumptions allow carrying out a limited number of reference CFD pre-computations that are used to subsequently determine relevant particle concentrations by superposition of contributions from the considered infectious occupants. More specifically, one main CFD simulation is required to determine the background flow field, considering the relevant boundary conditions associated to the considered ventilation scenario. Subsequently, simulations of particle dispersion can be performed by exploiting the available background field, which acts as a forcing term for the movement of particles (see section 2.4).

The information gathered from the CFD pre-computations is the concentration of saliva droplets at time t, released by the occupant n and arriving in front of the occupant j, normalized by the pulmonary ventilation rate of occupant n, i.e. $C'_{jn}(t)$. This information can be plugged into the analytical probabilistic model at the post-processing stage and, combined with information related to other relevant parameters of the model for the considered scenario, it allows determining relevant infection probability indices.

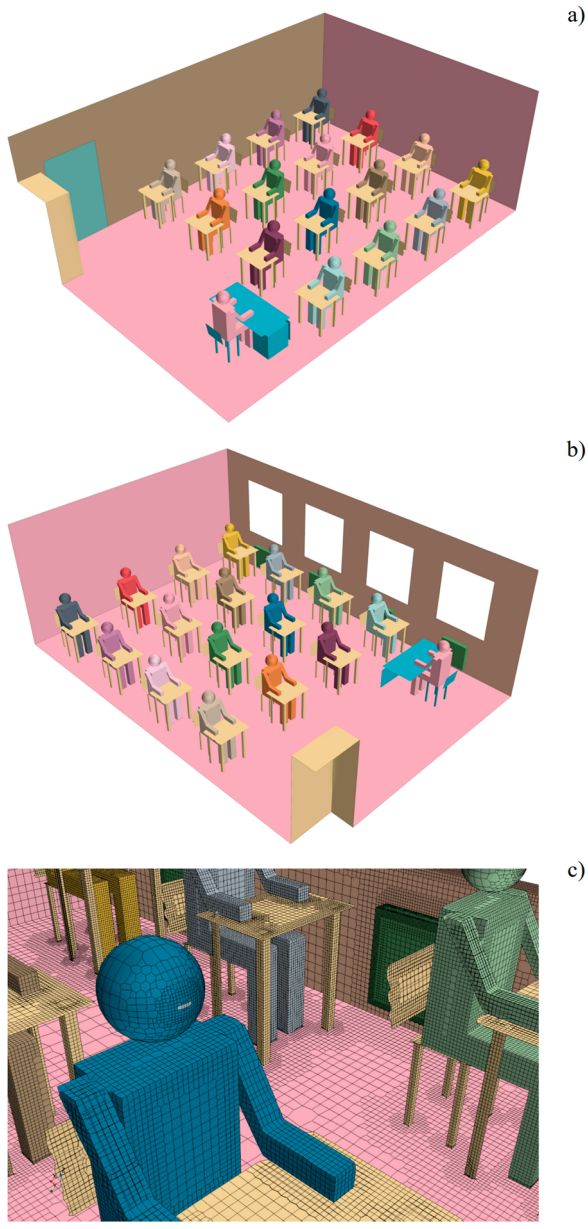

Figure 1. Views of the classroom computational domain: (a) open view from the outside, (b) open view from the access door, (c) detailed view of the mesh in the proximity of an occupant.

2.2. Quantitative infection model

The fundamental feature of quantitative infection models, as for the present work, is that the probability P that a susceptible individual develops the infection due to an

exposure of time length t depends on the quantity of airborne virus inhaled within the considered exposure time, i.e. the viral dose. Such models can be shortly referred to as dose–response models (e.g., Iddon et al. (2022), Sze To and Chao (2010), Watanabe et al. (2010)).

The approach presented in this work is generally applicable by using any dose–response model that provides the functional link between the individual probability of infection and the inhaled dose. However, to provide quantitative results for the example case study in section 3, use will be made of the Wells-Riley model (Riley, Murphy, and Riley 1978; Riley 2001), recast in the form of dose–response model (e.g., Iddon et al. (2022)), and this specific model is presented in the following.

The Wells-Riley model (Riley, Murphy, and Riley 1978; Riley 2001) is a classic model used to quantify the infection probability due to the airborne transmission of infectious, respiratory diseases (Noakes et al. 2006; Sze To and Chao 2010). The model was originally developed for estimating the infection probability in confined spaces, for tuberculosis and measles.

The Wells-Riley model (Riley, Murphy, and Riley 1978; Riley 2001) can be formulated in terms of inhaled viral dose, as follows (see also Iddon et al. (2022)):

$$P = 1 - e^{-c_i \cdot D(t)} \tag{1}$$

where P is the infection probability, $D(t)$ [RNA copies] is the viral dose inhaled within the exposure time t, and the infectivity coefficient c_i [(RNA copies)$^{-1}$] is a model parameter to link the inhaled viral dose and the infection probability according to the model (1). The form (1) corresponds to an exponential dose–response model (e.g., Watanabe et al. (2010)). It is noted that the original Wells-Riley model (Riley, Murphy, and Riley 1978; Riley 2001) is based on the concept of *quanta*, where *quanta* essentially correspond to the product $c_i \cdot D(t)$ in (1). According to the model (1), one quantum corresponds to $1/c_i$ viral copies and it is the viral dose leading to a probability of 63.2% to develop the infection. The customary application of the Wells-Riley model (Riley, Murphy, and Riley 1978; Riley 2001) relates, implicitly or explicitly, the coefficient c_i to the source of infection. In addition, a common value for c_i is generally assumed for a given viral species, irrespective of the characteristics of the susceptible person inhaling the virus. Nevertheless, it is reasonable to consider that the dependence between the inhaled viral dose and the infection probability, which is controlled by c_i in the model (1), may depend, at least in principle, both on the specific considered virus and on the susceptibility to infection of a specific person or community. Therefore, herein, it is proposed to consider that, in general, the coefficient c_i reflects the characteristics of the virus and the characteristics of the susceptible person inhaling the virus, thus c_i is conceptually associated with the susceptible individual inhaling the virus.

Quantitative infection models have been commonly applied under the assumption of well-mixing conditions within the considered confined space (e.g., Riley, Murphy, and Riley 1978; Buonanno, Morawska, and Stabile 2020a, 2020b; Iddon et al. 2022). When steady state and well-mixing conditions are assumed, the Wells-Riley model (Riley, Murphy, and Riley 1978; Riley 2001) takes the following form:

$$P = 1 - e^{-c_i \cdot \frac{N_{SOI} \cdot r}{Q_{vent}} \cdot p \cdot t} \tag{2}$$

where N_{SOI} is the number of individuals that are sources of infection (SOIs) in the room, r [RNA copies/h] is the rate of emission of viral copies for each SOI, Q_{vent} [m^3/h] is the room ventilation rate with germ-free air, p [m^3/h] is the pulmonary inhalation rate of each susceptible individual (SUI), and t [h] is the considered exposure time. The quantity $N_{SOI} \cdot r/Q_{vent}$ [RNA copies/m^3] represents the steady state concentration of viral copies in the air within the confined space. The quantity $p \cdot t$ [m^3] represents the total inhaled volume of air in the considered exposure time by the considered SUI, considering constant inhalation rate. Therefore, the inhaled does $D(t)$ within the exposure time corresponds to $(N_{SOI} \cdot r/Q_{vent}) \cdot p \cdot t$.

However, Noakes et al. (2006) show that risk assessments made using well-mixing assumption may significantly underestimate the real risk for people close to the infection source.

Therefore, the probabilistic approach proposed in the present investigation (section 2.3) is based on an unsteady local application of the Wells-Riley exponential dose–response model, where the viral dose inhaled by susceptible individuals is determined from the time-domain analysis of a so-called breath volume, located in close proximity in front of the mouth of the susceptible person.

According to Buonanno, Morawska, and Stabile (2020a, 2020b), the rate of emission of virus from each SOI, r, can also be reformulated as follows:

$$r = c_v \cdot v \cdot C \tag{3}$$

where c_v [RNA copies / mL of saliva] is the viral load associated with saliva droplets, v [m^3 of air/h] is the pulmonary exhalation rate from the infector, and the concentration C [mL of saliva / m^3 of air] takes into account the quantity of saliva per exhaled air volume.

In general, the concentration C appearing in equation (3) depends on the distribution of droplets size and on the overall number of particles per unit volume of

air. In this study, the droplets are modelled as spheres with diameter d_p, and the distribution of diameters is simplified by a discrete distribution for a finite set of n_d diameters (Buonanno, Stabile, and Morawska 2020b). Under these assumptions, the concentration C can be determined as follows:

$$C = \sum_{i=1}^{n_d} N(d_{p,i}) \cdot V_p(d_{p,i}) \tag{4}$$

where $N(d_{p,i})$ [droplets / m^3 of air] is the number of droplets having diameter $d_{p,i}$ per unit volume of air, and $V_p(d_{p,i})$ [mL of saliva / droplet] is the volume of a spherical saliva droplet of diameter $d_{p,i}$.

2.3. Probabilistic model for assessing infection probability indices

A probabilistic model is proposed to assess the infection susceptibility for the occupants of a confined space through the definition of probability indices. The model accounts for the probability that individuals may enter the room as infected (SOIs), for the actual arrangement of the classroom, for the different (fixed) positions that can be occupied by SOIs and SUIs and for the exposure time.

In the developed model, the inhaled viral dose within the exposure time t is determined for each susceptible occupant, considering the contributions from the assumed infected people (SOIs) in the room from the beginning of the assessment. The determination of the share of inhaled dose due to the emission from different SOIs is based on the assumption of superposition. From the fluid dynamics perspective, using superposition corresponds to the assumption of saliva droplets not affecting the airflow and not interacting with each other.

The presented approach provides indices related to infection probability starting from information regarding the dose inhaled by susceptible individuals due to the exhalations from infected occupants.

The main infection probability index that is determined from the presented model is the probability that at least one SUI gets infected considering an exposure time t, i.e. $P_{Sbl}(t)$. This probability is obtained by considering all possible combinations of infected/susceptible occupants in the room. Each of these combinations is referred to as a 'layout', it is conveniently defined by a binary vector $\boldsymbol{k}$ representing SUIs with zeros and SOIs with ones, and it is associated with a probability of occurrence $P_{\boldsymbol{k}}$ that depends on the probabilities $P_{I,j}$ that each occupant enters the room at time $t = 0$ as a SOI. By direct application of total probability theorem, the probability $P_{Sbl}(t)$ can be obtained by combining the probabilities $P_{\boldsymbol{k}}$ and the conditional infection probabilities $P_{Sbl|\boldsymbol{k}}(t)$. This latter probability is obtained considering the conditional infection probability for each occupant, $P_{Sbl,j|\boldsymbol{k}}(t)$. In turn, the probability $P_{Sbl,j|\boldsymbol{k}}(t)$ is obtained from the dose inhaled by each susceptible occupant, $D_{j|\boldsymbol{k}}(t)$, through an assumed dose–response model. In the case study presented in this paper (see section 3), the exponential dose–response model (1) is used. However, any other dose–response model providing the infection probability given the inhaled dose is equally applicable. The inhaled dose $D_{j|\boldsymbol{k}}(t)$ is obtained by superposition of relevant contributions $D_{jn}(t)$ due to each SUI in the room for the considered layout. Herein, the basic contributions $D_{jn}(t)$ are assumed to be obtained from CFD and particle tracking pre-calculations (see section 2.4). Nevertheless, the dose $D_{j|\boldsymbol{k}}(t)$ and/or the basic contributions $D_{jn}(t)$ can also be obtained from more simplified models (e.g., based on well-mixing assumption – see (2)). The probabilities obtained in the developed approach can also be used to determine the limiting infection probability for a hypothetical infinite exposure time, $P_{Sbl,lim}$. In addition, the probabilities obtained in the developed approach allow determining also the expected (mean) number of infection transmissions considering an exposure time t, both in terms of result conditional to a given layout, $\bar{N}_{Sbl|\boldsymbol{k}}(t)$, as well as in terms of marginal value $\bar{N}_{Sbl}(t)$.

Details of relevant formulae for the determination of the various quantities, and corresponding derivation, are reported in the following section 2.3.1.

2.3.1. Detailed derivation

In the following, an individual entering the room at $t = 0$ as not infected is referred to as a 'target'. Conversely, an individual entering the room at $t = 0$ as infected is referred to as a 'source'. A target is a susceptible individual, SUI, whereas a source is a SOI, i.e. an infected individual who contributes to the spreading of the virus. SUIs may get infected as a consequence of the exposure to the virus. Instead, SOIs, by definition, cannot 'get infected', because they already are. In the considered model, susceptible occupants getting infected are not considered infectious within the exposure time t, because the considered exposure time is assumed to be shorter than the incubation period.

A series of definitions that are relevant for the subsequent description of the probabilistic model are reported in Table 1.

For each scenario, the room layout is characterised by a combination of SUIs and SOIs among the available locations. Thus, a layout is identified by a binary vector $\boldsymbol{k}$ of indicators k_n ($n = 1, \ldots, N_P$), as follows:

$$k_n = \begin{cases} 0 & \textit{if the } n-\textit{th occupant is a SUI (a target)} \\ 1 & \textit{if the } n-\textit{th occupant is a SOI (a source)} \end{cases} \tag{5}$$

Table 1. Main definitions relevant to the description of the probabilistic model.

Quantity	Definition
N_P	Number of occupants, fixed at N_P corresponding locations during the exposure time.
$c_{v,n}$	Number concentration of virus copies in the saliva droplets exhaled by the source n, expressed as number of copies per mL of saliva.
$c_{i,j}$	Coefficient used in the Wells and Riley exponential dose-response model (see (1)) associated with the occupant j.
p_j	Inhalation volume flow rate of the occupant in the j-th position, expressed in m^3/h of inhaled air.
v_n	Exhalation volume flow rate of the occupant in the n-th position, expressed in m^3/h of exhaled air.
$C_{jn}(t)$	Concentration of saliva droplets at time t, released by the occupant n and arriving in front of the occupant j, expressed as mL of saliva per m^3 of air.
$C'_{jn}(t)$	Concentration of saliva droplets at time t, released by the occupant n and arriving in front of the occupant j, expressed as mL of saliva per m^3 of air, per unit exhalation flow rate of the occupant in the n-th position.
$D_{jn}(t)$	Viral dose inhaled by the occupant j within an exposure time t, due to saliva droplets exhaled by occupant n, expressed in RNA copies.
$\boldsymbol{k}$	Binary vector defining the scenario in terms of combination of SOIs and SUIs in the available locations (a 'layout').
$P_{\boldsymbol{k}}$	Probability of occurrence of a given layout $\boldsymbol{k}$.
$D_{j\|\boldsymbol{k}}(t)$	Viral dose inhaled by the occupant j within an exposure time t, for a given layout $\boldsymbol{k}$, expressed in RNA copies.
$P_{I,j}$	Probability that the occupant j is a source (i.e. already infected at $t = 0$)
$P_{SbI,j\|\boldsymbol{k}}(t)$	Probability that the occupant j gets infected considering an exposure time t, conditional to a given layout $\boldsymbol{k}$.
$P_{SbI,j}(t)$	Marginal probability that the occupant j gets infected considering an exposure time t.
$P_{SbI,j\|k_j=0}(t)$	Probability that the occupant j gets infected considering an exposure time t, conditional to entering the room as a target (i.e. a SUI) at $t = 0$.
$P_{SnI\|\boldsymbol{k}}(t)$	Probability that no SUI gets infected considering an exposure time t, conditional to a given layout $\boldsymbol{k}$.
$P_{SbI\|\boldsymbol{k}}(t)$	Probability that at least one SUI gets infected considering an exposure time t, conditional to a given layout $\boldsymbol{k}$, where $P_{SbI\|\boldsymbol{k}}(t) = 1 - P_{SnI\|\boldsymbol{k}}(t)$.
$P_{SnI}(t)$	Marginal probability that no SUI gets infected considering an exposure time t.
$P_{SbI}(t)$	Marginal probability that at least one SUI gets infected considering an exposure time t, where $P_{SbI}(t) = 1 - P_{SnI}(t)$.
$\bar{N}_{SbI\|\boldsymbol{k}}(t)$	Expected (mean) number of infection transmissions considering an exposure time t, conditional to a given layout $\boldsymbol{k}$.
$\bar{N}_{SbI}(t)$	Marginal expected (mean) number of infection transmissions considering an exposure time t.

Therefore, for a room with N_P locations, there are 2^{N_P} possible layouts. The 'layout 0' ($\boldsymbol{k} = \boldsymbol{0}$) refers to a situation where all the occupants are SUIs for $t = 0$. The 'layout 1' ($\boldsymbol{k} = \boldsymbol{1}$) identifies a situation where, for $t = 0$, all the occupants are SOIs.

Assuming the independence of the presence of sources among different available locations, and considering a layout $\boldsymbol{k}$, the probability of occurrence of the considered layout can be determined as

$$P_{\boldsymbol{k}} = \prod_{j=1}^{N_P} [(P_{I,j})^{k_j} \cdot (1 - P_{I,j})^{1-k_j}] \tag{6}$$

where the probability $P_{I,j}$ corresponds to the probability that an occupant in the j-th location enters the room at time $t = 0$ as infected, and it is associated with the overall diffusion of the infection in the considered reference communities.

The viral dose inhaled by the target occupant j within an exposure time t due to saliva droplets exhaled by the source occupant n is determined as

$$D_{jn}(t) = \begin{cases} \int_0^t c_{v,n} \cdot C_{jn}(\tau) \cdot p_j d\tau & \text{for } j \neq n \\ 0 & \text{for } j = n \end{cases} \tag{7}$$

It is noted that the definition of $D_{jn}(t)$ for $j = n$ as reported in (7) is conventional. However, since, by definition, a SOI cannot 'get infected', final results are not influenced by the actual definition used for $D_{jn}(t)$ when $j = n$.

The concentration $C_{jn}(t)$ in (7) can be determined from the corresponding normalized concentration $C'_{jn}(t)$ as follows

$$C_{jn}(t) = C'_{jn}(t) \cdot v_n \tag{8}$$

The terms $C'_{jn}(t)$ represent the link between the present probabilistic model and the pre-processing based on CFD and particle tracking. In fact, the normalized time-dependent concentrations $C'_{jn}(t)$ are pre-calculated by the combined CFD and particle tracking approach, and this is carried out only once. Afterwards, the whole probabilistic calculations are based on post-processing of such data, as described in the present section.

With reference to (7), it is noted that, for each generic occupant, by mass conservation, the value of inhalation and exhalation rates are the same, i.e.

$$p_h = v_h \; (h = 1, \ldots, N_P) \tag{9}$$

while the rates may differ among occupants. On the basis of (9), it would be possible to use a single symbol for both rates. However, two different symbols are retained in the description of the model with the intention of more clearly highlighting the part of formulation related to the 'source' individuals (exhalation rate, v_n) and the part of formulation related to the 'target' individuals (inhalation rate, p_j).

For a given layout $\boldsymbol{k}$, the determination of $D_{j|\boldsymbol{k}}(t)$ is based on the superposition of contributions from each source in the considered layout. Therefore,

$$D_{j|\boldsymbol{k}}(t) = \sum_q D_{jq}(t) \tag{10}$$

where q are the indices of sources in the considered layout, i.e. indices such that $k_q = 1$. Alternatively, taking into

account the definition of k_n (see (5)), $D_{j|\boldsymbol{k}}(t)$ can be equivalently rewritten as:

$$D_{j|\boldsymbol{k}}(t) = \sum_{n=1}^{N_P} D_{jn}(t) \cdot k_n \tag{11}$$

Targets (i.e. SUIs, $k_j = 0$) may get infected depending on the viral dose inhaled within the exposure time, whereas sources (i.e. SOIs, $k_j = 1$), by definition, cannot 'get infected'. As a result, the definition of the inhaled dose $D_{j|\boldsymbol{k}}(t)$ is relevant only for SUIs, i.e. when $k_j = 1$.

Assuming to use a generic dose–response model, the probability of infection can be determined as a function of the inhaled dose as follows

$$P_{SbI,j|\boldsymbol{k}}(t) = \begin{cases} 0 & \text{if } k_j = 1 \\ f_P(D_{j|\boldsymbol{k}}(t)) & \text{if } k_j = 0 \end{cases} \tag{12}$$

where the function $P = f_P(D)$ is, in general, the assumed dose–response model.

When the dose–response model is specifically defined according to (1), the infection probability for each SUI can be determined as follows

$$P_{SbI,j|\boldsymbol{k}}(t) = \begin{cases} 0 & \text{if } k_j = 1 \\ 1 - e^{-c_{i,j} \cdot D_{j|\boldsymbol{k}}(t)} & \text{if } k_j = 0 \end{cases} \tag{13}$$

where it is recalled that $k_j = 1$ if the occupant in the j-th position is a SOI (i.e. a source), whereas $k_j = 0$ if the occupant in the j-th position is a SUI (i.e. a target). It is highlighted that, to take into account possible differences in the characteristics of the occupants in terms of infection sensitivity to the inhaled virus, the coefficient $c_{i,j}$ is considered to be possibly dependent on the specific j-th target.

The marginal probability $P_{SbI,j}(t)$ can be obtained from the conditional probability $P_{SbI,j|\boldsymbol{k}}(t)$ and the probability of occurrence of each possible layout, $P_{\boldsymbol{k}}$, by considering all possible layouts, as follows

$$P_{SbI,j}(t) = \sum_{\boldsymbol{k}} P_{SbI,j|\boldsymbol{k}}(t) \cdot P_{\boldsymbol{k}} \tag{14}$$

The marginal probability $P_{SbI,j}(t)$ implicitly accounts also for cases where the occupant in the j-th position is infected at $t = 0$, i.e. those cases such that $k_j = 1$. In such cases, by definition, the occupant in the j-th position is a SOI and cannot 'get infected'. Hence, $P_{SbI,j|\boldsymbol{k}}(t) = 0$ as consistently defined in (12)/(13).

In the assessment of a room arrangement, it is also relevant to assess the probability of getting infected due to the stay in the confined space, when the occupant entered the room as non-infected (i.e. as a SUI). Therefore, for an occupant in the generic j-th location, it is meaningful to assess the probability of getting infected, conditional to the fact that the occupant entered the room in a susceptible state at $t = 0$, i.e. conditional to $k_j = 0$. Herein, this probability is denoted as $P_{SbI,j|k_j=0}(t)$ and it can be determined as follows:

$$P_{SbI,j|k_j=0}(t) = \frac{\sum_{\boldsymbol{k}:k_j=0} (P_{SbI,j|\boldsymbol{k}}(t) \cdot P_{\boldsymbol{k}})}{\sum_{\boldsymbol{k}:k_j=0} P_{\boldsymbol{k}}} \tag{15}$$

The denominator in equation (15) represents the probability of having a layout where the j-th occupant is a SUI (i.e. a target), i.e. the probability that the occupant of the j-th position entered the room at $t = 0$ as a target. At the same time, by definition (see (12)/(13)), $P_{SbI,j|\boldsymbol{k}}(t) = 0$ whenever the j-th occupant is a source ($k_j = 1$). Therefore:

$$\sum_{\boldsymbol{k}:k_j=0} (P_{SbI,j|\boldsymbol{k}}(t) \cdot P_{\boldsymbol{k}}) = \sum_{\boldsymbol{k}} (P_{SbI,j|\boldsymbol{k}}(t) \cdot P_{\boldsymbol{k}}) = P_{SbI,j}(t) \tag{16}$$

In addition, the probability that the j-th occupant entered the room as a SUI (i.e. a target) can be linked to the probability $P_{I,j}$ that the occupant entered the room as a SOI (i.e. a source), as follows:

$$\sum_{\boldsymbol{k}:k_j=0} P_{\boldsymbol{k}} = 1 - P_{I,j} \tag{17}$$

By combining equations (15)–(17), the probability $P_{SbI,j|k_j=0}(t)$ can be equivalently determined as:

$$P_{SbI,j|k_j=0}(t) = \frac{P_{SbI,j}(t)}{1 - P_{I,j}} \tag{18}$$

The probability that no SUI gets infected for a given layout $\boldsymbol{k}$ considering an exposure time t can be determined as:

$$P_{SnI|\boldsymbol{k}}(t) = \prod_{j:k_j=0} (1 - P_{SbI,j|\boldsymbol{k}}(t)) \tag{19}$$

In (19), the product considers positions of the layout $\boldsymbol{k}$ occupied by SUIs ($k_j = 0$). However, if the occupant of the generic j-th location is a source, it is $P_{SbI,j|\boldsymbol{k}}(t) = 0$ by definition (see (12) /(13)). Thus, $P_{SnI|\boldsymbol{k}}(t)$ in (19) can be equivalently rewritten as:

$$P_{SnI|\boldsymbol{k}}(t) = \prod_{j=1}^{N_P} (1 - P_{SbI,j|\boldsymbol{k}}(t)) \tag{20}$$

The marginal probability that no target gets infected considering an exposure time t, $P_{SnI}(t)$, can be determined from the combination of the conditional probability $P_{SnI|\boldsymbol{k}}(t)$ and the probability of occurrence of each different layout, $P_{\boldsymbol{k}}$, as:

$$P_{SnI}(t) = \sum_{\boldsymbol{k}} P_{SnI|\boldsymbol{k}}(t) \cdot P_{\boldsymbol{k}} \tag{21}$$

Therefore, the probability that at least one target gets infected considering an exposure time t, $P_{SbI}(t)$, can be

determined as:

$$P_{Sbl}(t) = 1 - P_{Snl}(t) = 1 - \sum_{\boldsymbol{k}} P_{Snl|\boldsymbol{k}}(t) \cdot P_{\boldsymbol{k}}$$
$$= \sum_{\boldsymbol{k}} (1 - P_{Snl|\boldsymbol{k}}(t)) \cdot P_{\boldsymbol{k}} = \sum_{\boldsymbol{k}} P_{Sbl|\boldsymbol{k}}(t) \cdot P_{\boldsymbol{k}} \quad (22)$$

where use has been made of the fact that $\sum_{\boldsymbol{k}} P_{\boldsymbol{k}} = 1$ and $P_{Sbl|\boldsymbol{k}}(t) = 1 - P_{Snl|\boldsymbol{k}}(t)$.

The probability $P_{Snl}(t)$ can be used as a merit figure, i.e. as an index to be kept as high as possible, for the classification of a given room arrangement (in terms of ventilation, occupation, layout of furniture, etc.) with respect to the limitation of the propagation of an airborne viral infection. Conversely, for the same purpose, the probability $P_{Sbl}(t)$ can be used as a demerit figure, i.e. as an index to be kept as small as possible.

If, for a given layout $\boldsymbol{k}$, there is at least one target (a SUI) and at least one source (a SOI) in the room (namely $\boldsymbol{k} \neq \boldsymbol{0}$, $\boldsymbol{1}$) and if the arrangement allows saliva droplets to reach a target from a source, then, there is at least one function $D_{jn}(t)$ increasing with the exposure time t. As a result, under these conditions, the probability that at least one occupant will get infected in the limit of an infinite exposure time is equal to 1.

For the special cases $\boldsymbol{k} = \boldsymbol{0}$ and $\boldsymbol{k} = \boldsymbol{1}$, it is $P_{Sbl|\boldsymbol{k}}(t) = 0$ at any time. For $\boldsymbol{k} = \boldsymbol{0}$, all occupants are SUIs (i.e. targets) and cannot get infected because there are no SOIs (i.e. sources) in the room. For $\boldsymbol{k} = \boldsymbol{1}$, all occupants are SOIs (i.e. sources), therefore they are already infected at $t = 0$ and, by definition, they cannot 'get infected'.

The limit of $P_{Sbl}(t)$ as the exposure time tends to infinity, $P_{Sbl,lim}$, can be determined as

$$P_{Sbl,lim} = \lim_{t \to +\infty} P_{Sbl}(t)$$
$$= \lim_{t \to +\infty} \sum_{\boldsymbol{k}} P_{Sbl|\boldsymbol{k}}(t) \cdot P_{\boldsymbol{k}}$$
$$= \lim_{t \to +\infty} \left[\sum_{\boldsymbol{k} \neq \boldsymbol{0},\boldsymbol{1}} (P_{Sbl|\boldsymbol{k}}(t) \cdot P_{\boldsymbol{k}}) + \sum_{\boldsymbol{k} = \boldsymbol{0},\boldsymbol{1}} (P_{Sbl|\boldsymbol{k}}(t) \cdot P_{\boldsymbol{k}}) \right]$$
$$= \sum_{\boldsymbol{k} \neq \boldsymbol{0},\boldsymbol{1}} (1 \cdot P_{\boldsymbol{k}}) + \sum_{\boldsymbol{k} = \boldsymbol{0},\boldsymbol{1}} (0 \cdot P_{\boldsymbol{k}}) = \sum_{\boldsymbol{k} \neq \boldsymbol{0},\boldsymbol{1}} (1 \cdot P_{\boldsymbol{k}})$$
$$= \sum_{\boldsymbol{k}} (1 \cdot P_{\boldsymbol{k}}) - \sum_{\boldsymbol{k} = \boldsymbol{0},\boldsymbol{1}} (1 \cdot P_{\boldsymbol{k}})$$
$$= 1 - (P_{\boldsymbol{k}=\boldsymbol{0}} + P_{\boldsymbol{k}=\boldsymbol{1}})$$
$$= 1 - \left(\prod_{j=1}^{N_P} (1 - P_{I,j}) + \prod_{j=1}^{N_P} (P_{I,j}) \right) \quad (23)$$

It is noted that the limit probability $P_{Sbl,lim}$ from (23) corresponds to the probability that there are at least a SOI and at least a SUI in the room, under the additional assumption that the room arrangement is such to allow saliva droplets to reach at least a SUI from at least a SOI and that the dose–response model provides a unit probability of getting infected for an infinite inhaled dose. According to these assumptions, it can be noticed that the limit probability $P_{Sbl,lim}$ does not depend on the specific details of the used dose–response model. $P_{Sbl,lim}$ depends only on the probabilities $P_{I,j}$, i.e. the probabilities for the occupants of entering the room at $t = 0$ as a SOI.

Additional merit or demerit metrics can also be used for the assessment of given scenarios. For instance, Iddon et al. (2022) used the expected number of transmissions, with correspondingly associated proportion of population newly infected.

According to the approach presented herein, the expected (mean) number of infection transmissions conditional to a given layout considering an exposure time t, $\bar{N}_{Sbl|\boldsymbol{k}}(t)$, can be determined as follows:

$$\bar{N}_{Sbl|\boldsymbol{k}}(t) = \sum_{j:k_j=0} P_{Sbl,j|\boldsymbol{k}}(t) \quad (24)$$

Also in this case, noting that, by definition (see (12)/(13)), $P_{Sbl,j|\boldsymbol{k}}(t) = 0$ whenever the j-th occupant is a source ($k_j = 1$), it follows that:

$$\bar{N}_{Sbl|\boldsymbol{k}}(t) = \sum_{j=1}^{N_P} P_{Sbl,j|\boldsymbol{k}}(t) \quad (25)$$

Therefore, the marginal expected (mean) number of transmissions considering an exposure time t, $\bar{N}_{Sbl}(t)$, can be determined as

$$\bar{N}_{Sbl}(t) = \sum_{\boldsymbol{k}} \bar{N}_{Sbl|\boldsymbol{k}}(t) \cdot P_{\boldsymbol{k}} = \sum_{j=1}^{N_P} P_{Sbl,j}(t) \quad (26)$$

where use has also been made of (16).

The proportion of population newly infected, as defined by Iddon et al. (2022), can be determined by dividing $\bar{N}_{Sbl|\boldsymbol{k}}(t)$ and $\bar{N}_{Sbl}(t)$ by the total number of occupants N_P, to obtain a conditional or marginal quantity, respectively. Accordingly, and taking into account (25) and (26), the proportion of population newly infected represents the average value of $P_{Sbl,j|\boldsymbol{k}}(t)$ or $P_{Sbl,j}(t)$, respectively, across the occupants.

For the presented approach, $c_{v,n}$, $c_{i,j}$, p_j and v_n are considered as deterministic parameters. Therefore, all obtained results are conditional to the assumed values of these parameters. However, the framework can be extended to explicitly account also for a probabilistic description of these parameters. This can be done by

introducing further averaging using specified distributions for these additional parameters among SOIs and SUIs. In this respect, it is worth noting the example of the probabilistic model by Iddon et al. (2022), where the viral load is considered as a random variable with given distribution.

As a complement to the present section, Appendix 5 shows an example application, only from the point of view of the probabilistic model, to a simplified case of a room with three occupants.

2.4. Model of particle dispersion

The combined use of CFD simulations and discrete particle tracking allows evaluating how infectious droplets disperse through the indoor air.

The discrete particle model has been already applied to study the dispersion of virus and bacteria in confined spaces (Zhang, Tu, and Ling 2008; Casagrande and Piller 2020). The respiratory aerosols are composed of inner particles and outer mucus (Feng, Zhang, and Lan 2012). The evaporation of the latter influences the aerosols' dispersion and deposition. However, the shrinkage time from the original respiratory aerosols to particles is rapid (about 0.5 s), especially for particles whose size is smaller than 20 µm (Nicas, Nazaroff, and Hubbard 2005). Therefore, in the present study, heat transfer and evaporation related to saliva droplets have been neglected, and respiratory aerosols are modelled as particles with constant size. The low volumetric loading ratio of respiratory aerosol also suggests that the assumption of one-way coupling is sound for indoor airflows, as the particle motion essentially does not affect the background airflow (Kuerten 2016). Furthermore, the particle-particle collisions can be neglected due to the large inter-particle distance. According to Lai and Nazaroff (2000), the low velocity of indoor airflows supports the assumption that the airborne particles experience a plastic and adhesive collision against the solid walls. In addition, the collision is assumed to be instantaneous, the presence of the interstitial fluid is neglected and the surface roughness is ignored. The thermophoretic transport can also be neglected in the modelling of indoor airflows, due to the size of the airborne particles and due to the airflow velocities.

The kinematic and dynamic equations governing the motion of a particle are as follows (Kuerten 2016):

$$\frac{\mathrm{d}\boldsymbol{x}_p}{\mathrm{d}t} = \boldsymbol{u}_p \tag{27}$$

$$\rho_p \cdot \frac{\mathrm{d}\boldsymbol{u}_p}{\mathrm{d}t} = -\nabla p + \frac{1}{2} \cdot \rho \cdot C_D \cdot \frac{A_p}{V_p} \cdot |\boldsymbol{u} - \boldsymbol{u}_p| \cdot (\boldsymbol{u} - \boldsymbol{u}_p) + (\rho_p - \rho) \cdot \boldsymbol{g} + \rho \cdot C_a \cdot \left(\frac{\mathrm{D}\boldsymbol{u}}{\mathrm{D}t} - \frac{\mathrm{d}\boldsymbol{u}_p}{\mathrm{d}t} \right) \tag{28}$$

where $\boldsymbol{x}_p$ and $\boldsymbol{u}_p$ are the particle position and velocity vector, respectively. The symbols A_p and V_p in (28) represent the cross-flow area and the volume of a particle, respectively. With reference to the right hand side of equation (28):

- $\boldsymbol{u}$ is the velocity vector of the background flow field, and $\frac{D\boldsymbol{u}}{Dt}$ corresponds to its material derivative, i.e. $\frac{D\boldsymbol{u}}{Dt} = \frac{\partial \boldsymbol{u}}{\partial t} + \boldsymbol{u} \cdot \nabla \boldsymbol{u}$;
- The first term is the force acting on a particle due to a local pressure gradient in the surrounding fluid. It is noted that the pressure p denotes the absolute pressure without hydrostatic contribution;
- The second term describes the drag force, where the drag coefficient C_D is determined according to Schiller's model (Schiller 1935);
- The third term combines the effect of weight and buoyancy. It is noted that the buoyancy term appears because the pressure p in the first term does not contain the hydrostatic contribution;
- The fourth term represents so-called added mass effects, which are related to the acceleration of the fluid and of the particle. Since particles are considered to be spherical, an added mass coefficient $C_a = 0.5$ is used.

In principles, particles may experience also lift-type forces (Rubinow and Keller 1961; Saffman 1965). However, in the considered scenarios, the Reynolds number for shear flow which is used to determine the shear lift force, in accordance with Saffman (1965), is significantly smaller than 1 throughout the flow domain (as reported in the Supplementary Material for the scenario 20 of the case study – see section 3), suggesting that the shear lift force can be safely neglected. Moreover, the rotation lift force associated to the Magnus effect caused by a relative rotation between the particle and the fluid (Rubinow and Keller 1961), is neglected in the present simulations due to the very small values of the rotational Reynolds number (as reported in the Supplementary Material for the scenario 20 of the case study – see section 3).

The particle tracking is simulated by the numerical integration of the ODE system (27)-(28) for each particle. To this purpose, the required background flow field $\boldsymbol{u}$ is obtained from CFD computations. The Eulerian model for the air flow and for the temperature distribution relies on the Reynolds-Averaged Navier-Stokes (RANS) turbulence closure. Only the long-term averaged (Reynolds-averaged) components of all flow quantities are explicitly solved for, while the turbulent fluctuations are linked

to their long-term counterparts via a turbulence model. The long-term quantities attain a steady state that is reached by advancing in time an unsteady model (an unsteady model is used merely for computational purposes, because it provides easier convergence of the iterative solvers). The applied particle model is discussed in detail in the Supplementary Material.

All CFD simulations are carried out by means of Simcenter STAR-CCM + ®, version 2021.1.3 by Siemens Digital Industries Software. Validation of the numerical model is reported in Appendix 1. The realizable k-ε model is used to simulate the 3D turbulent airflow field, and relevant information is detailed in Appendix 2.

3. Case study

The case study focuses on a single school classroom, and its corresponding internal airflow field is predicted by CFD simulations. A mesh-sensitivity analysis is reported in Appendix 3.

In the case study, the target is to consider possible infections due to SARS-CoV-2. In this respect, six scenarios, differing only for the ventilation strategy, are compared and ranked according to the probability $P_{Sbl}(t)$ that at least one susceptible occupant develops the infection considering an established exposure time (see section 2.3).

From CFD (Lagrangian) simulations, the concentration of saliva droplets is calculated within control volumes directly located in front of the nose and of the mouth of each occupant. This information is used as input for the probabilistic model, in accordance with the methodology described in section 2.3.

Additional information regarding the present case study are provided as Supplementary Material in the online version of this article, as follows:

- The full geometrical model of the classroom (see section 3.1 hereinafter), in 3dm format;
- Details of the setup of CFD simulations used to determine the background flow field and to simulate particles dispersion (see sections 3.3 and 3.4 hereinafter);
- A code in MATLAB language, with associated input data, to reproduce results of the probabilistic post-processing (see section 3.5 hereinafter).

3.1. Main characterizing data

The case study and associated numerical model used for the present investigation are developed in accordance with the available guidelines and regulations for arrangement and operation of classrooms in the Italian education system from the point of view of indoor comfort and energy efficiency (Italian Parliament 2005; Ministry of Economic Development et al. 2015; President of Italian Republic 2013), accounting for regulations on the containment of COVID-19 pandemic (Italian Parliament 2020, 2021). The case study is an adaptation from a real classroom located in a secondary school building in the province of Trieste (North-Eastern Italy), whose construction dates back to the period 1946−1960, and the analysis is carried out considering winter season.

The classroom sizes a gross area of 8.67 m × 6.00 m = 52.02 m^2, with a net indoor height equal to 3.00 m. Four windows are open on the wall, facing outside, each having a transparent surface of 1.68 m^2. A visual characterization of the classroom is provided in Figure 1. The classroom layout encompasses a total of 17 occupants: 16 students and one teacher. The four green blocks below the windows sills in Figure 1 represent the classroom heaters.

Heaters are a common heating system in Italian school buildings. Moreover, in most classrooms clean air is exclusively provided by natural ventilation (Fuoco et al. 2015). Therefore, the condition where all windows and doors are closed (airtight) and the classroom heaters are active, can be considered as a reference (most severe) condition as for the risk of infection. Furthermore, all occupants are assumed not to wear face masks. The contamination predicted by the present simulations can be easily rescaled to represent the case where the infected occupants wear face masks: in this case, a reduction of the viral dose inhaled by a SUI can be evaluated by applying filtration efficiency coefficients to exhalation and inhalation acts (Dai and Zhao 2020).

The inter-personal distance resulting from the selected number of occupants reflects relevant literature and regulatory indications: 1.80 m^2 in-plan area per occupant in Primary and Secondary School buildings from Italian Interministerial Decree 18 December 1975, and minimum inter-personal distance of 1.5-2.0 m from Welsch et al. (2021) or 1.0 m from Italian National Law No. 35 of 22 May 2020.

Furthermore, all the fomites within the school building must be frequently sterilized and, in any case, sterilization should be carried out every day before the beginning of the lessons. Dispensers of cleansing gel/solution are expected to be made available in every teaching and working space within the school. Therefore, infection due to contacts with contaminated surfaces is neglected.

The boundary conditions assigned in the simulation consider internal walls, door, ceiling and floor as adiabatic surfaces, while external walls are characterized by a thermal transmittance $U_{OP} = 1.25$ W m^{-2} K^{-1}. The thermal transmittance of the windows, including frames, is set to $U_W = 5.00$ W m^{-2} K^{-1}. These parameters have been

set accounting for a diffuse condition in Italian educational buildings that are operating since the early 1960s and have not yet been subject to major refurbishment interventions. As previously reported, four heaters are located under each window sill of the considered classroom. Water circulating through heaters is set at 65 °C in winter.

Five portable air cleaners (PACs) are assumed to be located in the classroom, close to adiabatic internal walls. Three PACs are located at the back of the last row of student seats. The remaining two PACs are positioned close to the wall behind the teacher and close to the classroom corners. PACs are placed on small supporting tables, and each supporting table has a height of 0.45 m from the floor (see Figure 2 reported later in this section).

Following Feng, Zhang, and Lan (2012), the temperature of students' and teacher's body is set at 31 °C. The occupants' mouth are the sources of water droplets for infected subjects.

In the determination of the background flow field through CFD calculations, occupants' breathing is neglected. This allows attaining a steady background flow field within the classroom that significantly improves the computational efficiency during calculations.

Instead, occupants' breathing is considered in Lagrangian particle tracking simulations, in terms of a mean exhalation velocity that is used as ejection velocity of particles. The mean exhalation velocity is assumed equal to 1.0 m/s in accordance with both nasal and mouth breathing determined through experimental campaigns (Girardin, Bilgen, and Arbour 1983; Tang et al. 2013).

According to Adams (1993) the pulmonary ventilation rates, averaged between males and females, are equal to 0.49, 0.54, 1.38, 2.35 and 3.30 $m^3\ h^{-1}$ for five different activity levels (resting, standing, light exercise, moderate exercise, and heavy exercise, respectively). Naftali et al. (1998) assume for their CFD simulations of airflow through the nasal cavity that normal adults under rest conditions breath a tidal volume of about 0.5 litres with a breathing rate of 15 min^{-1}. For the present investigation, relevant pulmonary ventilation rates (p,v) have been assumed to be ranging from 0.5 $m^3\ h^{-1}$ to 1.25 $m^3\ h^{-1}$, consistently with the low activity level of the occupants during class hours and with their young age (excluding, possibly, the teacher).

In the present investigation, the distribution of the diameter of droplets forming the exhaled aerosol is reflected by $N(d_{p,i})$ in equation (4), and it was taken from Buonanno, Stabile, and Morawska (2020b).

With reference to the SARS-CoV-2 viral load, data available in literature suggest a concentration of virus copies in exhaled saliva droplets, c_v, which is variable during the evolution of the disease. Prentiss, Chu, and Berggren (2022) report literature data ranging from 10^2 to 10^{10} RNA copies/mL, while Buonanno, Stabile, and Morawska (2020b) report that c_v attains values of 10^8-10^9 RNA copies/mL of saliva in the first disease days, increasing up to 10^{11} RNA copies/mL of saliva in later stages (Buonanno, Stabile, and Morawska 2020b; Pan et al. 2020).

Regarding the coefficient of infectivity, c_i, which is used to link the inhaled dose and the infection probability, Buonanno, Stabile, and Morawska (2020b) adopt c_i in

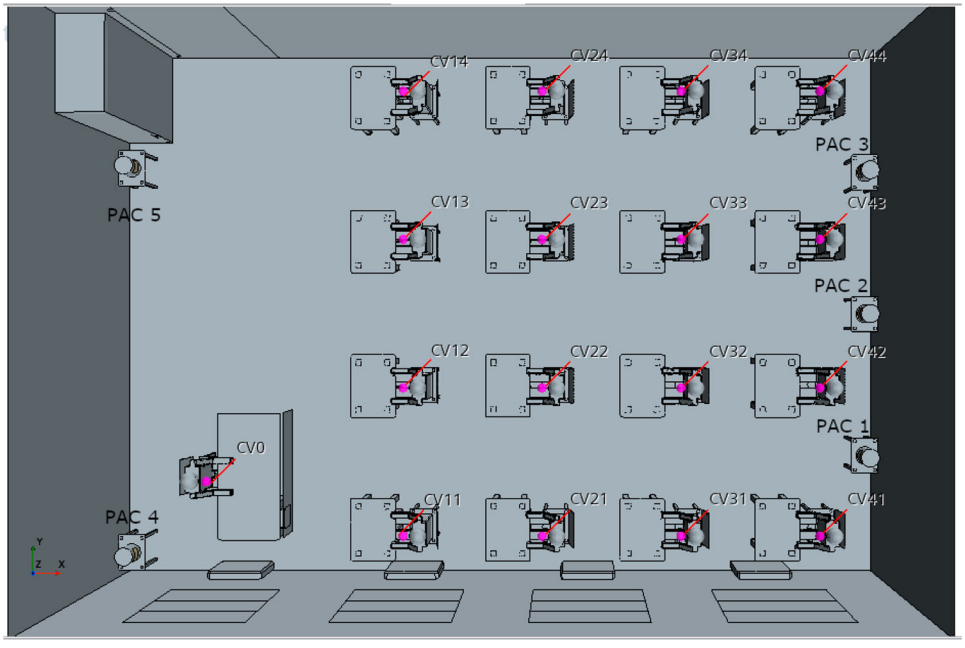

Figure 2. Position of control volumes associated to each occupant within the classroom, and PACs identification number.

the range 0.01–0.1 (RNA copies)$^{-1}$, based on the data by Watanabe et al. (2010) for SARS-CoV-1, which is claimed to have similar characteristics to SARS-CoV-2 (van Doremalen et al. 2020). Abbas and Gursel Dino (2022) adopt $c_i = 1/280$ (RNA copies)$^{-1}$, also referring to data reported by Watanabe et al. (2010). In a recent study, Prentiss, Chu, and Berggren (2022) use information about five COVID-19 superspreading events to estimate values of the characteristic number of virions needed to induce infection, N_0 (which can be linked to the inverse of c_i herein), of about 300–2000 virions. The values of N_0 provided by Prentiss, Chu, and Berggren (2022) are obtained from the application of a dispersion model for the airborne virus, based on the well-mixing assumption and accounting for different mechanisms of decay of the virus (gravitational settling, virus inactivation, attenuation and dilution). The reference model parameter used by Prentiss, Chu, and Berggren (2022) include the breathing rate and the concentration of viral copies in saliva droplets. This latter is assumed constant throughout all the considered events and equal to $c_v = 10^7$ RNA copies/mL of saliva. Abbas and Gursel Dino (2022), based on the experimental study by Leung et al. (2020), assume an emission rate r (see equation (3)) of 3.54×10^4 virus particles per hour, for their numerical investigation about the spreading of airborne SARS-CoV-2 infection in a classroom.

Data in literature indicate wide ranges for parameters required for quantitative infection modelling, such as pulmonary ventilation rates (p,v) and coefficients c_v and c_i. Recognizing (see equations (2) and (3)) that these parameters play their role in the Wells-Riley model through the product $S_q = r \cdot c_i = c_v \cdot v \cdot C \cdot c_i$, which is named 'quanta emission rate' by Prentiss, Chu, and Berggren (2022), it has been decided to assume $c_v = 10^{9.5}$ RNA copies/mL of saliva and $c_i = 10^{-1.5}$ (RNA copies)$^{-1}$, which lead to values of S_q per index patient of $\sim 120\,h^{-1}$. Prentiss, Chu, and Berggren (2022), for the events considered in their study, calculate S_q for the cases of virus emission by speaking (range $136\,h^{-1}$–$757\,h^{-1}$, average $461\,h^{-1}$) and by breathing (range $3\,h^{-1}$–$17\,h^{-1}$, average $10\,h^{-1}$). Therefore, the value $\sim 120\,h^{-1}$ associated with the parameters used in the present investigation can be considered (heuristically) consistent with the young age of most of the occupants of the considered classroom, who spend part of the exposure time listening and part talking, i.e. in an intermediate state between breathing and speaking. For comparison, Prentiss, Chu, and Berggren (2022) report scenario-averaged values of S_q for an event occurring in a Korean fitness centre ($152\,h^{-1}$) and for three events associated with bus rides of different durations ($133\,h^{-1}$, $36\,h^{-1}$, $62\,h^{-1}$), all with one index patient.

Based on the reported information, Table 2 summarizes the parameters used for the model in the present case study.

The assessment is carried out for six scenarios that differ in terms of activation/flow-rate of PACs and in terms of airtightness of the windows. Specific details regarding the considered scenarios are provided in section 3.2. At the same time, some common conditions are assumed for all scenarios addressed in the study, namely: all the classroom occupants (students and teacher) are sitting and remain seated, heaters are active, and indoor surfaces and indoor air are sterile at the initial time instant ($t = 0$).

To evaluate the concentration of droplets, spherical control volumes with radius of 5 cm are positioned in front of the face of each occupant, at 1.07 m and 1.15 m above ground, for students and teacher, respectively. The position of the considered control volumes is shown in Figure 2. The figure reports also the position and the identification number of each PAC.

The definition of relevant values for the probability $P_{I,j}$ (see (6)) was based on the combination of information related to the average daily number of infected people, the proportion of infected people based on age and the associated reference populations. Two age groups have been considered, namely, 6-19 years, relevant to students, and 20-69 years, relevant to the teacher. First, the average daily number of infected people was determined starting from daily values of infected people registered in Italy for the whole population, i.e. irrespective of age, in the period from 1st May 2020 to 30th April 2022 (INFN 2022). Then, the distribution of age in positive people (INFN 2022) was used to estimate the proportion of infected people for each considered age group. These two data have been used to estimate the average

Table 2. Main simulation parameters.

Parameter	Units	Reference value for simulations	Notes
cv	RNA copies/mL of saliva	$10^{9.5}$	Based on range 10^8–10^{11}
ci	(RNA copies)$^{-1}$	$10^{-1.5}$	Based on range 0.01–0.1
p,v	m^3 h^{-1}	0.875	Based on range 0.50–1.25
N	droplets/cm3	0.236 ($d_p = 0.80$ µm), 0.068 ($d_p = 1.80$ µm), 0.007 ($d_p = 3.50$ µm), 0.011 ($d_p = 5.50$ µm)	Corresponding to (see (4)): C = $1.386 \cdot 10^{-6}$ mL of saliva / m^3 of air
Heaters' operation temperature	°C	65	

Table 3. Probabilities $P_{I,j}$ for each age group, and relevant data used in the estimations.

Age group [years]	6–19	20–69
Average daily number of infected people for all ages (Period: 1st May 2020 – 30th April 2022)	461′706	461′706
Proportion of infected people by age group [%]	15.33	67.19
Estimated average daily number of infected people by age group	70′780	310′233
Italian population by age group	7′717′150	38′114′518
Estimated $P_{I,j}$ [%]	0.9172	0.8139

daily number of infected people for each considered age group. Finally, the obtained values were divided by the overall Italian population corresponding to each group as of 1st January 2022 (ISTAT 2022). Relevant data and obtained values of $P_{I,j}$ for the two considered age groups are reported in Table 3.

In the application of the probabilistic model in section 2.3 for the present case study, all relevant calculation parameters have been set the same for all occupants, without distinguishing between students and teacher. The only exception is the probability $P_{I,j}$, which was set differently for the students and for the teacher, in accordance with data in Table 3.

3.2. Definition of ventilation scenarios

The assessment of infection probability indices for the considered classroom has been performed for six different ventilation scenarios.

In a set of three ventilation scenarios, PACs are switched off, whereas they are switched on, with different flow rates, in the remaining three scenarios. The supply vents of the PACs are modeled as mass-flow inlet boundaries, while the suction vents of the PACs are treated as mass-flow outlets, where the pressure is prescribed to attain the same mass-flow rate released through the PACs supply vents. Lee et al. (2022) have shown that portable air cleaning devices with HEPA filters classed not lower than H13 have an extremely high purification efficiency. Therefore, in this study, the purification efficiency of PACs, when switched on, is assumed to be 100%, meaning that all droplets are assumed to be removed from the air passing through the PACs. When switched on, each PAC is assumed to deliver a flow rate corresponding to 160 m^3/h or 320 m^3/h, when operating at low or high flow rate, respectively. When switched-on, PACs are assumed to release a heat rate of 50 W each, which is considered to be uniformly distributed over their surface. The main information regarding PACs operation is summarised in Table 4.

In addition to considering different operational states for PACs, the considered six scenarios also address the effect of different windows characteristics. The contribution of windows to the ventilation scenarios is linked to their air permeability, and relevant information in this respect have been taken from the specifications by the CEN standard EN 12207 (European Committee for Standardization 2016). Accordingly, three alternative conditions are considered, corresponding to different windows performance classes. Specifically, one ideal condition was considered where windows are perfectly air-tight. Two additional conditions have been also considered, with windows of Class 3 and Class 2, where airflows of about 8.1 m^3/h and 14.4 m^3/h, respectively, are supplied through each window. These three alternative conditions adequately represent different cases of Italian educational heritage, corresponding to recently built buildings (ideally air-tight) or buildings dating back to 1990s (Class 3) and 1960s (Class 2).

Table 4. PACs parameters for the considered ventilation scenarios.

Parameter	Units	Reference value	Notes
Flow rate through suction and supply vent	m3/h	0; 160; 320	switched off, low flow-rate, high flow-rate – Values for single PAC

The six scenarios considered in this case study are reported in Table 5, together with the corresponding scenario ID. The scenario ID depends on the activation of PACs and, if active, on their imposed flow-rate and on the level of classroom envelope airtightness ensured by windows. Specifically, the ID is composed of two digits, in the form ID = PW, where:

- The first digit P refers to the operation of PACs. It is equal to 0 for PACs switched off, to 1 for PACs operating at low flow-rate and to 2 for PACs operating at high-flow rate;
- The second digit W refers to the level of airtightness of the windows. It is equal to 0 for air-tight windows, it is equal to 1 for weakly permeable windows and it is equal to 2 for highly-permeable windows.

In the comparison of the ventilation scenarios, which will be reported in section 3.5, two reference exposure

Table 5. Considered ventilation scenarios.

ID	Description
00	PACs switched off, air-tight windows
01	PACs switched off, weakly permeable windows
02	PACs switched off, highly-permeable windows
10	PACs operating at low flow-rate, air-tight windows
20	PACs operating at high flow-rate, air-tight windows
21	PACs operating at high flow-rate, weakly permeable windows

times will be considered, namely 1 h and 5 h. In case of 5-hour exposure time, an intense ventilation, lasting 10 min, is assumed to be applied every hour. This is intended to reflect the behaviour that is expected in the management of classrooms in case of risk of infection, where periodic ventilation of the room is obtained by, e.g., opening the windows.

From a numerical perspective, particle dispersion simulations are carried out for an exposure time of 1 h, during which the dispersion of the aerosol exhaled by the SOIs is tracked by the Lagrangian model. Instead, data for the 5-hour exposure are generated at a post-processing stage, by joining relevant time traces corresponding to five identical 1-hour exposure time windows. In performing the joining of data, it is assumed that the room is ventilated during each 10-minute hourly break. Consequently, it is assumed that, for the first 50 min of each hour, the SUIs accumulate viral dose according to the reference 1-hour Lagrangian simulation and they do not accumulate additional viral doses during the 10-minute break.

The considered ventilation scenarios aim to verify the applicability and to demonstrate the usefulness of the proposed probabilistic assessment technique. Nevertheless, they are not entirely representative of the actual ventilation that could be expected in a real classroom, where the windows would likely be opened by the occupants whenever the air quality degraded below an acceptable limit. For instance, in the reference scenario 00 in Table 5 with airtight door and windows, assuming an emission rate of CO_2 of 0.55 gCO_2/min per person, an outdoor concentration of CO_2 of 400 p.p.m. and under well-mixing conditions, the concentration of CO_2 within the classroom would rise to about 2500 p.p.m. in one hour. By comparison, Di Gilio et al. (2021) measure CO_2 concentrations in 11 naturally ventilated classrooms in Southern Italy and show that the mean concentration of CO_2 is about 1750 p.p.m. in all classrooms and always lower than 4000 p.p.m.

3.3. Example patterns of airflow field

This section provides some examples regarding the simulated airflow in the scenarios 00 and 20. Figure 3 shows the distribution of the vertical velocity component w on three plane sections, for the example scenarios. As for the scenario 00 (Figure 3a), the regions of relatively large w correspond to the thermal plumes induced by the buoyancy forces in the surroundings of warm surfaces (heaters and occupants). The thermal plumes are less evident in the scenario 20 (Figure 3b), as the horizontal jets generated by the air cleaners induce a predominantly horizontal velocity field, while impairing the formation of thermal

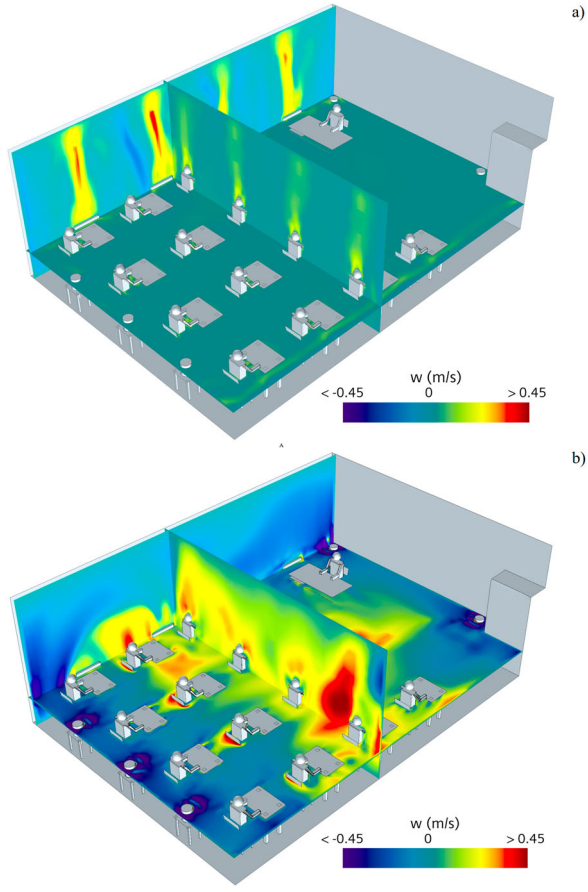

Figure 3. Vertical velocity component w on three plane sections. (a) scenario 00 with inactive PACs, (b) scenario 20 with active PACs.

plumes. Regions of relatively high vertical velocity are caused by the interaction of the nearly horizontal jets generated by the air cleaners with the obstacles present in the classroom.

3.4. Example patterns of infected aerosol

This section provides some examples regarding the distribution of infected aerosol in the scenarios 00 and 20. In the reported examples, a single SOI placed at position 11 exhales contaminated droplets, assuming a mean breathing rate $v = 0.875\ m^3\ h^{-1}$ (see Table 2). Based on the mean rate v and the concentration C of saliva droplets (see Table 2), the mean exhalation rate of saliva can be determined as $v \cdot C = 1.2 \cdot 10^{-6}$ mL of saliva / h.

The example isosurfaces shown in Figure 4 correspond to a non-dimensional mass-concentration of saliva droplets in air of $5{\cdot}10^{-4}$ at time t = 60 s after the initiation of the release. In this respect, the mass-concentration of saliva droplets is scaled by the reference concentration C_{ref} defined as

$$C_{ref} = \rho_p \cdot C \tag{29}$$

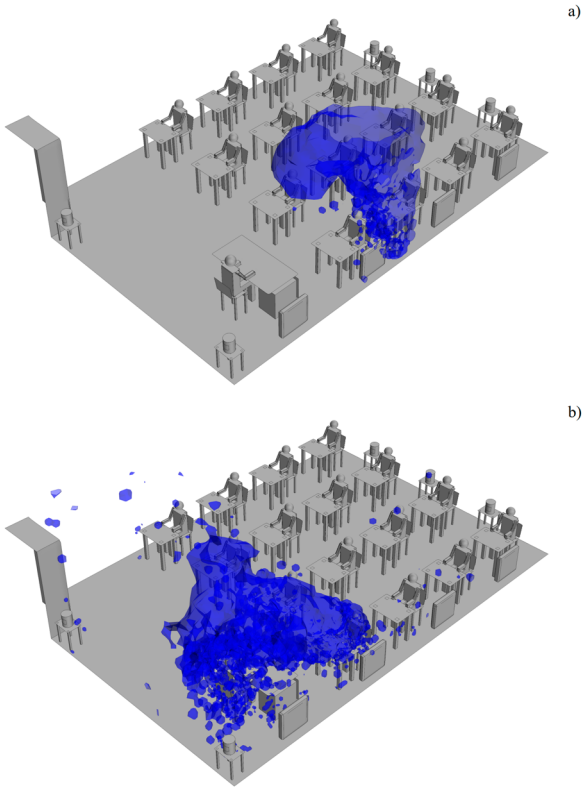

Figure 4. Example isosurfaces of non-dimensional mass-concentration of saliva droplets at simulation time t = 60s corresponding to $5{\cdot}10^{-4}$. Exhalation rate corresponding to 0.875 $m^3\ h^{-1}$. The source of infection is the student in position 11. (a) scenario 00 with inactive PACs, (b) scenario 20 with active PACs.

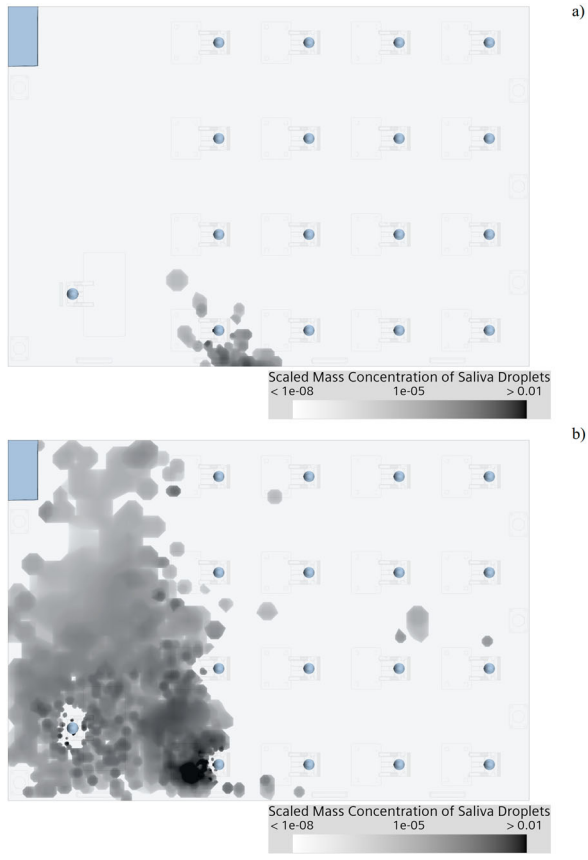

Figure 5. Distribution of non-dimensional mass-concentration of saliva droplets on a horizontal plane section at the height of control volumes for students (1.07 m from floor level), at simulation time t = 60s. Exhalation rate corresponding to 0.875 $m^3\ h^{-1}$. The source of infection is the student in position 11. (a) scenario 00 with inactive PACs, (b) scenario 20 with active PACs.

where C [mL of saliva / m^3 of air] is the concentration of saliva per exhaled air volume (see (4)), while ρ_p denotes the density of saliva which is taken as $\rho_p = 0.001$kg/mL.

If PACs are switched off (scenario 00 – Figure 4a), the dispersion of the plume of contaminated saliva droplets is governed by buoyancy. As a result, the droplets move mainly upwards rather than horizontally, and the teacher is less directly involved. Conversely, for the scenario 20 (Figure 4b), the emitted plume of infected droplets is pulled towards the nearest PAC and runs over the teacher, increasing the likelihood of infection for the teacher.

Figure 5 shows the distribution of non-dimensional mass concentration of saliva droplets on a horizontal plane section at the height of control volumes for students (1.07 m from floor level), 60 s after the SOI's first release of particles (i.e. at simulation time t = 60s). In the scenario 00 (Figure 5a) the contaminant is entrapped in a rising thermal plume (see Figure 3a) and it does not significantly disperse horizontally. Conversely, in the scenario 20 (Figure 5b) the contaminant moves with the airflow, predominantly induced by the air cleaners, and higher concentrations at breathing height are evident throughout the whole part of the classroom located in front of the SOI.

Figure 6 shows the time dependence of the accumulated viral dose emitted from the student in position 11 and inhaled either by the teacher (Figure 6a and b) and by the student in position 31 (Figure 6c and d), considering both the case of 1-hour and 5-hour exposure time. The activation of the PACs at the highest considered flow-rate (scenario 20) determines a significant reduction of the accumulated dose for the student in position 31 compared to the scenario 00, while the opposite occurs for the teacher. This is due to the fact that, when the PACs are active (scenario 20), the cloud of high viral concentration shown in Figure 4 is drawn towards the teacher, and this causes a higher viral concentration in front of the teacher itself, compared to the condition where no PAC is active (scenario 00).

3.5. Assessment of infection probability indices and ranking of ventilation scenarios

The probability index $P_{Sbl}(t)$ that at least one SUI gets infected considering a given exposure time t (see section

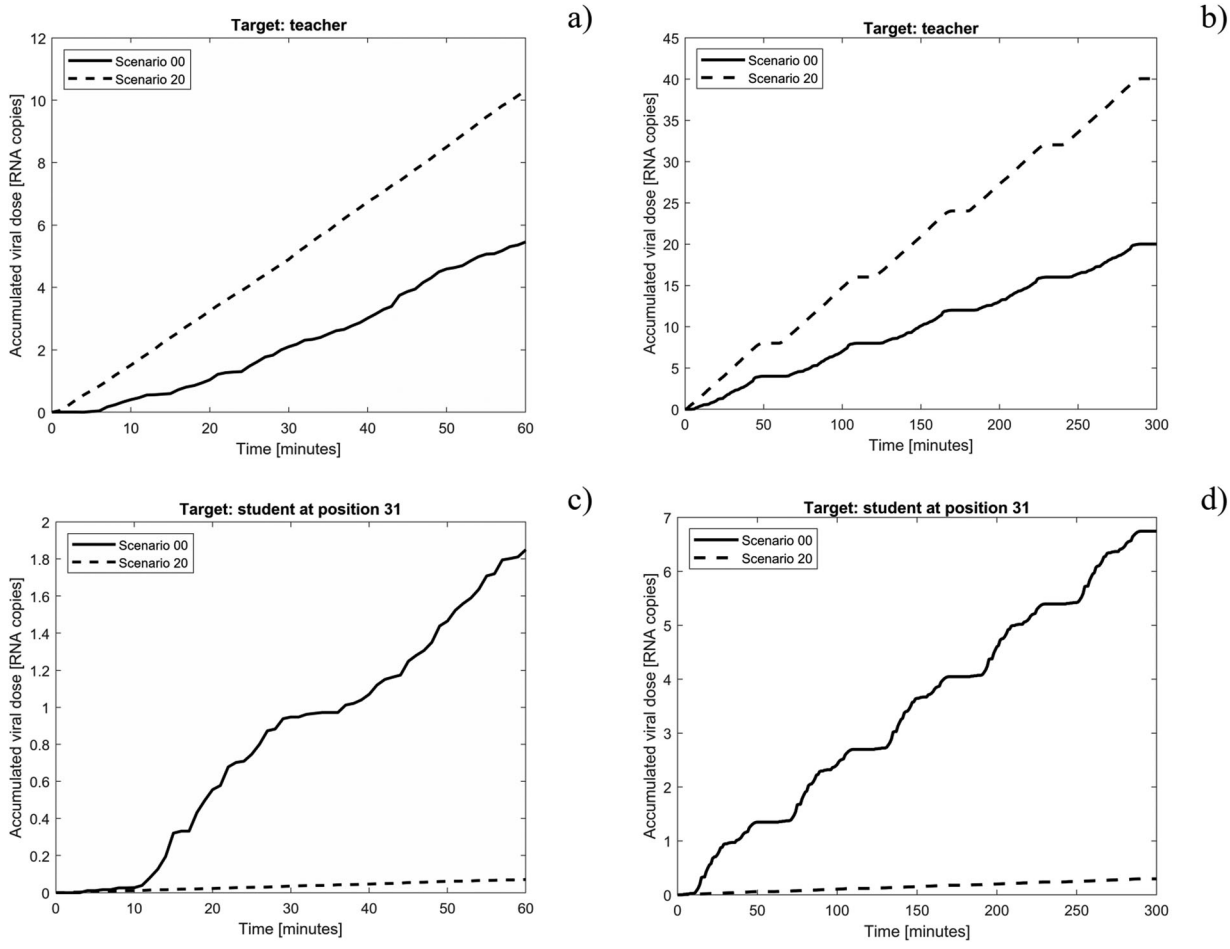

Figure 6. Time histories of accumulated viral dose inhaled by the teacher (exposure time: (a) 1 h, (b) 5 h) and by the student at position 31 (exposure time: (c) 1 h, (d) 5 h), when the student at position 11 is the only SOI, with $p = 0.875$ m^3 h^{-1}, $c_v = 10^{9.5}$ RNA copies/mL of saliva. The considered scenarios are scenario 20 (dashed line) and scenario 00 (solid line), according to Table 5.

2.3) has been calculated for the scenarios reported in Table 5 and considering two reference exposure times, namely 1 h and 5 h (this latter with 10 min intense ventilation every hour – see section 3.2).

As already described, for the application of the probabilistic model from section 2.3, all relevant calculation parameters (see section 3.2) have been set the same for all occupants, without distinguishing between students and teacher, with the exception of $P_{I,j}$. The probability $P_{I,j}$ is an exception, because it was set differently for the students and for the teacher, in accordance with data in Table 3.

In addition, it is valuable to look at the obtained outcomes for each scenario also in relative terms, by taking into account the limit probability $P_{SbI,lim}$ (see (23)). The value of the probability $P_{SbI,lim}$ is the same for all scenarios, under the additional assumption that, for each scenario, the virus removal effectiveness of the ventilation strategy is less than 100%. A rational relative effectiveness of each ventilation scenario, $\varepsilon_v(t)$, can be defined as follows :

$$\varepsilon_v(t) = 1 - \frac{P_{SbI}(t)}{P_{SbI,lim}} \tag{30}$$

From the expression of $P_{SbI,lim}$ in (23), and from the assumed values of $P_{I,j}$ for students and teacher (see Table 3), $P_{SbI,lim}$ for the considered cases is obtained as

$$P_{SbI,lim} = 14.4\% \tag{31}$$

The index $\varepsilon_v(t)$ is considered to be an indicator that may be more representative than the absolute probability index $P_{SbI}(t)$. The considered improvement of $\varepsilon_v(t)$ over $P_{SbI}(t)$ comes from the fact that $\varepsilon_v(t)$ takes into account the normalization by the limiting probability $P_{SbI,lim}$, where $P_{SbI,lim}$ is representative of effects on infection probability indices coming from external factors, i.e. terms $P_{I,j}$, see (23).

The obtained results for $P_{SbI}(t)$, $\varepsilon_v(t)$ and $\bar{N}_{SbI}(t)$ are reported in Table 6, considering $p = 0.875$ m^3 h^{-1}, $c_v = 10^{9.5}$ RNA copies/mL of saliva, $c_i = 10^{-1.5}$ (RNA copies)$^{-1}$. The table reports also the maximum of $\bar{N}_{SbI|\boldsymbol{k}}(t)$ across all layouts $\boldsymbol{k}$.

Table 6. Evaluation metrics for the considered scenarios depending on exposure time t: probability $P_{Sbl}(t)$ that at least one SUI gets infected, effectiveness index $\varepsilon_v(t)$, expected number of infection transmissions $\bar{N}_{Sbl}(t)$, and maximum conditional expected number of infection transmissions $\bar{N}_{Sbl|\boldsymbol{k}}(t)$ across all layouts $\boldsymbol{k}$. The ranking of the scenarios is also reported, based on $P_{Sbl}(t)$ for 5-hour exposure time.

Exp. time [h]	Scen.00 P_{Sbl} [%]; ε_v [%]; $\bar{N}_{Sbl}$; max($\bar{N}_{Sbl\|\boldsymbol{k}}$)	Scen.01 P_{Sbl} [%]; ε_v [%]; $\bar{N}_{Sbl}$; max($\bar{N}_{Sbl\|\boldsymbol{k}}$)	Scen.02 P_{Sbl} [%]; ε_v [%]; $\bar{N}_{Sbl}$; max($\bar{N}_{Sbl\|\boldsymbol{k}}$)	Scen.10 P_{Sbl} [%]; ε_v [%]; $\bar{N}_{Sbl}$; max($\bar{N}_{Sbl\|\boldsymbol{k}}$)	Scen.20 P_{Sbl} [%]; ε_v [%]; $\bar{N}_{Sbl}$; max($\bar{N}_{Sbl\|\boldsymbol{k}}$)	Scen.21 P_{Sbl} [%]; ε_v [%]; $\bar{N}_{Sbl}$; max($\bar{N}_{Sbl\|\boldsymbol{k}}$)
1	10.32; 28.39; 0.209; 6.63	6.20; 56.96; 0.0942; 4.11	5.91; 59.00; 0.0912; 4.06	5.24; 63.63; 0.0676; 3.17	3.63; 74.78; 0.0412; 2.43	3.25; 77.47; 0.0367; 1.89
5	13.53; 6.12; 0.574; 11.36	11.66; 19.07; 0.301; 9.52	10.66; 26.02; 0.305; 9.49	10.97; 23.87; 0.216; 7.27	9.01; 37.49; 0.138; 5.93	7.93; 44.94; 0.117; 4.47
Ranking based on $P_{Sbl}(t)$ for $t = 5h$	VI	V	III	IV	II	I

Results in Table 6 show that the ventilation scenarios with active PACs operating at high flow rate (scenarios 20 and 21) are the most effective in limiting the infection probability. The highest values for the parameter $\varepsilon_v(t)$ and the lowest values for P_{Sbl} are attained for the scenario 21, the one with the largest overall ventilation among the considered scenarios.

The proposed methodology allows addressing infection probability indices also on a local basis, i.e. depending on the position within the classrooms. Herein, this probability is referred to as $P_{Sbl,j}(t)$ (see (14)). From results in Table 6, it can be seen that the worst and best scenarios in terms of probability $P_{Sbl}(t = 5\ h)$ are scenarios 00 and 21, respectively. This result is consistent with intuition, as the scenarios 00 and 21 represent the conditions of minimum (absent) and maximum ventilation, respectively. Figure 7a and b show $P_{Sbl,j}(t = 5\ h)$ for these extreme scenarios, while Figure 7c represents the probability index $P_{Sbl,j}(t)$ for the scenario 01. Figure 7 also shows results of $P_{Sbl,j}(t = 5\ h)$ normalized by the corresponding value for scenario 00 (see Figure 7d for scenario 21 and Figure 7e for scenario 10).

The spatial distribution of the probability index $P_{Sbl,j}(t)$ allows identifying the seats within the classroom that could be potentially associated with the highest likelihood of infection for specific ventilation scenarios. Comparing Figure 7a and b, referring to 5-hour exposure time, the positive effect of the increase of ventilation is evident.

Scenarios 01 and 21, where a Class 3 permeability is assumed for the windows according to CEN standard EN 12207 (European Committee for Standardization 2016), are representative of a significant part of Italian school building heritage (Almeida, Ramos, and Pereira 2017; Secchi et al. 2017; Stabile et al. 2016). Among the two scenarios, scenario 21 provides information regarding the effect of installation of PACs. Therefore, it is valuable to look at the difference between the probability indices $P_{Sbl,j}(t)$ for scenario 01 (reference) and scenario 21 (retrofitting), as shown in Figure 8. Figure 8a shows absolute differences of infection probability indices between scenario 21 and scenario 01, while Figure 8b reports the same differences normalised by using the values of scenario 01 as reference.

In the scenario 01, the region of maximum infection probability extends in close proximity and in front of the door, due to the convergence of the airflow towards the only outflow surface from the classroom. The pattern for the scenario 21 is markedly different: the region of maximum $P_{Sbl,j}(t)$ surrounds the student 43, who intercepts an air stream of high particle concentration drawn towards the PACs 2 and 3 (see Figure 2), lying just behind and on either side of student 43 (see Figure 2).

Overall, the PACs induce a reduction of the infection probability indices for all sitting positions. A reduction of infection probability indices is observed also when the windows are considered permeable.

As anticipated in section 2.3, the infection probability index $P_{Sbl}(t)$ can be used as a demerit figure to rank different ventilation scenarios. Equivalently, the companion complementary probability index $P_{Snl}(t) = 1 - P_{Sbl}(t)$ can be used as a merit figure, for the same purpose. From an engineering design perspective, ranking of different ventilation scenarios could be considered as a fundamental purpose.

It is finally necessary to remember that the ranking of ventilation scenarios is linked to the assumed values of model parameters. These parameters are associated with an intrinsic level of uncertainty, and different values of model parameters may lead to different outcomes. Therefore, it is interesting to investigate also the robustness of the obtained ranking with respect to variations in the assumed values of calculation parameters. This aspect is addressed in Appendix 4, where the six considered

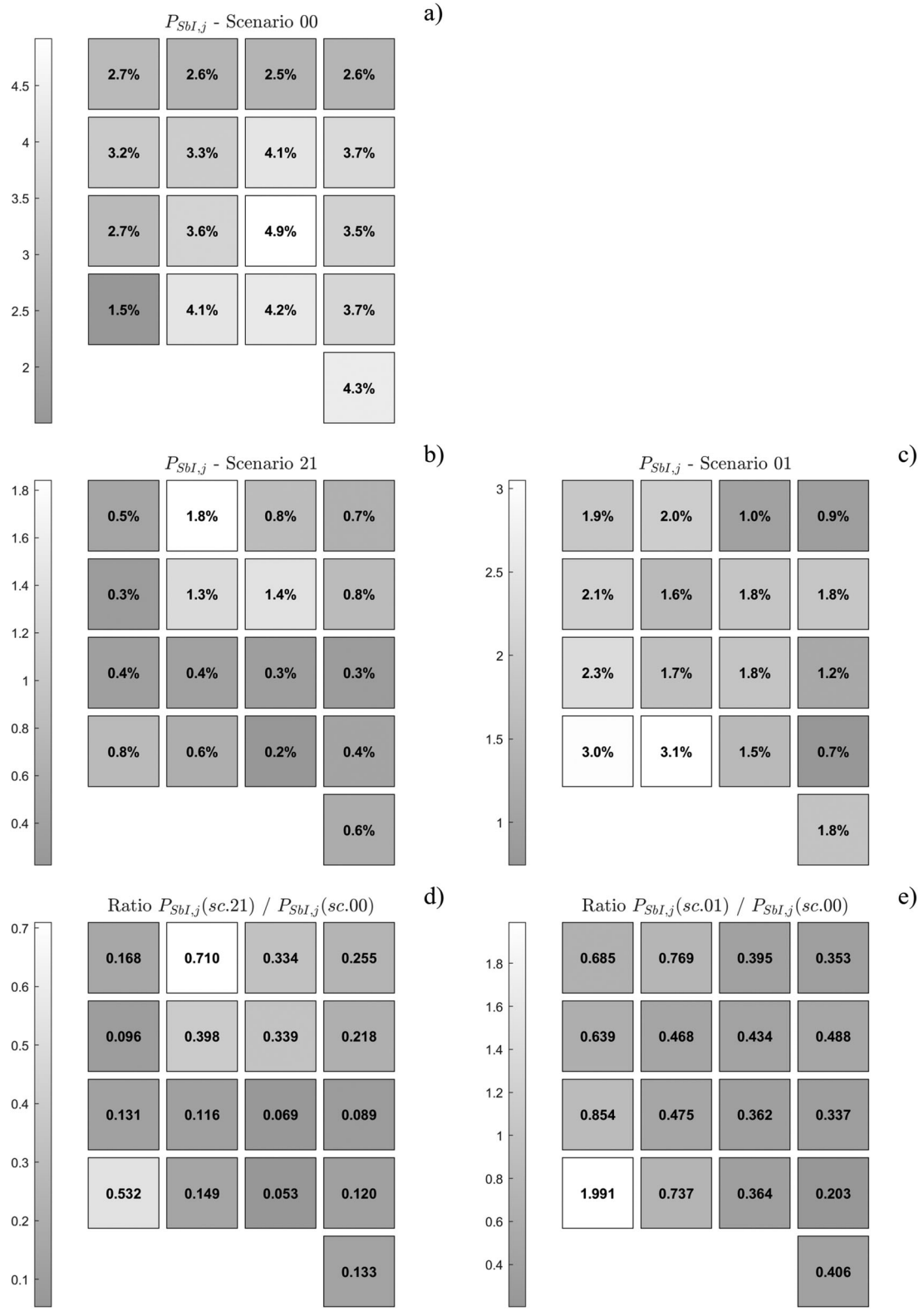

Figure 7. Infection probability indices $P_{SbI,j}$ considering 5-hour exposure time. Absolute values: (a) scenario 00, (b) scenario 21, (c) scenario 01. Values normalized by results for scenario 00: (d) scenario 21, (e) scenario 01.

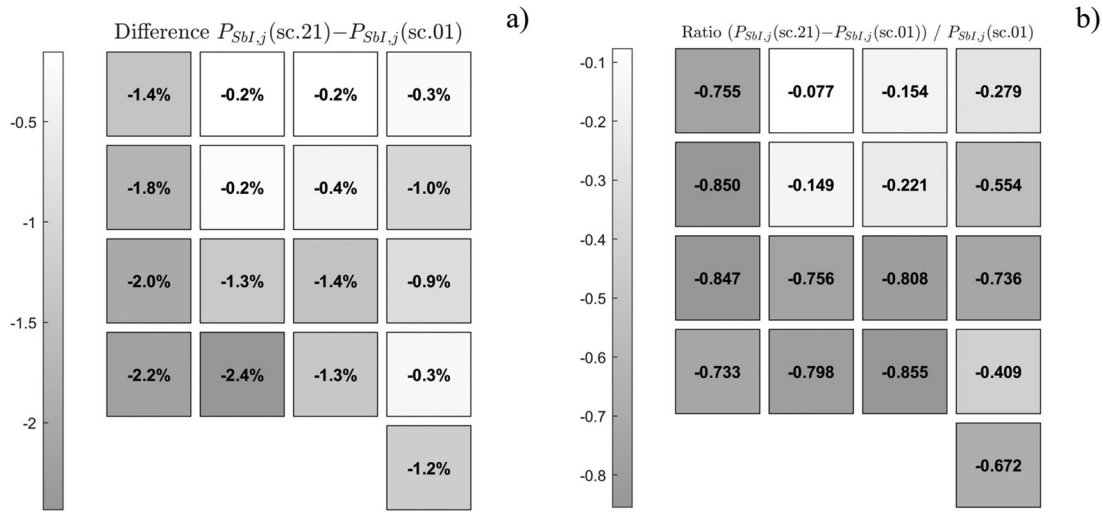

Figure 8. Differences of infection probability indices $P_{SbI,j}$ between scenario 01 and scenario 21, considering 5-hour exposure time: (a) absolute values, (b) values normalized by $P_{SbI,j}$ for scenario 01.

ventilation scenarios (Table 5) have been ranked considering the 5-hour exposure time and considering variations in model parameters.

4. Conclusions

The containment of the spreading of airborne diseases requires implementing some risk control options, such as increasing the distance between individuals and reducing the effect of the exhaled airflows by wearing face masks or other personal protective equipment. Nevertheless, the infection probability may still be high when people stay in relatively close contact for a sufficiently long exposure time in confined spaces. In view of the above, the first aim of this work has been the development of an efficient methodology for the probabilistic assessment of the likelihood of infection in confined spaces which are continuously occupied for relatively long periods. The approach is based on a combination of a limited number of CFD pre-calculations for droplets dispersion and an analytical post-processing of the obtained data, exploiting superposition, to define relevant indices of infection probability. The separation between CFD pre-computations and subsequent analytical post-processing also allows quick re-assessment of scenarios in case of changes in relevant calculation parameters, e.g., due to changes in the epidemiological situation, or in case there is an interest in assessing the effects of face masks, etc.

The present framework is applicable to generic confined spaces, although the probabilistic procedure has been tested on a case study of a naturally-ventilated classroom in the winter season. Most classrooms in the Italian school buildings are naturally ventilated. While a weak ventilation is continuously guaranteed by the permeability of windows and fixtures, most of the air renewal is attained by opening the windows, usually when the indoor air quality has excessively worsened due to the increase of CO_2 concentration. During the winter season, the windows remain closed for most of the lesson time, facilitating the accumulation of biological pollutants, as bacteria and viruses, within the classrooms. The various ventilation scenarios considered in the presented case study differ by the permeability of the windows and by the possible activation of five Portable Air Cleaners (PACs). The proposed methodology has been used to rank the considered ventilation scenarios based on calculated infection probability indices. The obtained results confirm the intuition that an increase of ventilation and/or air filtration reduces the overall likelihood of infection. The most effective ventilation scenarios among those tested were those with PACs operating at high flow rate. Results also suggest a similarity in terms of performance between the PACs activation at a low flow rate and a condition of high permeability of the windows. In addition, the capabilities of the proposed approach allowed to observe that the positive effect of increasing ventilation is not uniform within the space. This is a consequence of the fact that the operation of PACs induces a global modification of the background flow field, which affects the dispersion of the infected aerosol within the room.

From a methodological perspective, the presented approach could be used, in principle, for absolute assessment as well as for relative, i.e. comparative, assessment. At the same time, absolute assessment is more challenging than relative assessment. In fact, modelling assumptions and simplifications tend to have a more significant effect on absolute assessment results compared to results from relative assessment. To be confident with absolute assessment results, it is necessary to achieve a sufficient level of confidence on each part of the modelling,

which typically requires application experience, revisions, updates, validations, etc. Relative assessment, especially when it is aimed at providing a ranking among difference alternatives, tend to be more robust with respect to modelling assumptions and simplifications. The presented case study proved the approach to be practical for assessing alternative ventilation scenarios in terms of their associated infection probability indices. Furthermore, a specific analysis showed the robustness of the results of ranking among different ventilation scenarios, with respect to assumptions in some of the input parameters.

It is also worth adding a note on the relation between the presented approach and simpler approaches, based on, e.g., well-mixing assumption, from the point of view of design and/or analysis. Compared to simpler approaches, the presented approach provides more detailed information, but it also requires more computational effort and input parameters. Despite the presented approach is much more efficient than repeated brute force CFD-based simulations, the required computation effort can still represent a limitation of the methodology. From a practical perspective, this means that the computational effort associated with the use of CFD simulations limits the possibility of using such an approach for wide parametric studies. Therefore, results of CFD computations with subsequent probabilistic post-processing provide probabilistic indices that are essentially conditional to those parameters that cannot or are impractical to be varied and to be considered in probabilistic terms. At the same time, the impact of this limitation depends on the specific intended use, and the presented approach can be considered as a complementary tool with respected to simpler approaches. For instance, in a multi-tier design and analysis framework, simpler approaches may be more suitable for initial wide preliminary screening, based on global parameters, while the presented approach may be more suitable for subsequent detailed analyses on a selected set of scenarios.

The modularity of the presented framework makes it naturally open to further developments and improvements related to the basic components (CFD model, dose–response model, probabilistic post-processing), while keeping the overall methodological approach. A transversal topic that would be worth being addressed, is the introduction of uncertainty for those parameters that have been considered as deterministic in the presented study. In this respect, the introduction of uncertainty in parameters that are relevant only to the probabilistic post-processing stage is relatively straightforward, as this essentially requires further averaging and the post-processing is computationally fast. The introduction of uncertainty in parameters that affect the results of CFD pre-calculations requires more efforts, due to the need to cope with the practical limits related to computational time.

Disclosure statement

No potential conflict of interest was reported by the author(s).

Funding

This work was partially supported by the University of Trieste: [Grant Number FRA2020 Research Fund].

Declaration of competing interest

The authors declare that they have no known competing financial interests or personal relationships that could have appeared to influence the work reported in this paper.

Data availability statement

The data that support the findings of this study are available from the corresponding author upon reasonable request.

References

Abbas, G. M., and I. Gursel Dino. 2022. "COVID-19 Dispersion in Naturally-Ventilated Classrooms: a study on Inlet-Outlet Characteristics." *Journal of Building Performance Simulation* 15: 656–677. https://doi.org/10.1080/19401493.2022.2063946.

Adams, W. C. 1993. Measurement of Breathing Rate and Volume in Routinely Performed Daily Activities, Final Report.

Almeida, R. M. S. F., N. M. M. Ramos, and P. F. Pereira. 2017. "A Contribution for the Quantification of the Influence of Windows on the Airtightness of Southern European Buildings." *Energy and Buildings* 139: 174–185. https://doi.org/10.1016/j.enbuild.2017.01.012.

Asadi, S., N. Bouvier, A. S. Wexler, and W. D. Ristenpart. 2020. "The Coronavirus Pandemic and Aerosols: Does COVID-19 Transmit via Expiratory Particles?" *Aerosol Science & Technology* 54: 635–638. https://doi.org/10.1080/02786826.2020.1749229.

Atkinson, J., Y. Chartier, C. L. Pessoa-Silva, P. Jensen, Y. Li, and S. Wing-Hong. 2009. *Natural Ventilation for Infection Control in Health-Care Settings*. Canberra (AU): World Health Organization.

Bartolucci, A., A. Templeton, and G. Bernardini. 2022. "How Distant? An Experimental Analysis of Students' COVID-19 Exposure and Physical Distancing in University Buildings." *International Journal of Disaster Risk Reduction* 70: art. 102752, 1–10. https://doi.org/10.1016/j.ijdrr.2021.102752.

Blocken, B., T. van Druenen, A. Ricci, L. Kang, T. van Hooff, P. Qin, L. Xia, et al. 2021. "Ventilation and air Cleaning to Limit Aerosol Particle Concentrations in a gym During the COVID-19 Pandemic." *Building and Environment* 193: art. 107659, 1–16. https://doi.org/10.1016/j.buildenv.2021.107659

Bruinen de Bruin, Y., A. S. Lequarre, J. McCourt, P. Clevestig, F. Pigazzani, M. Zare Jeddi, C. Colosio, and M. Goulart. 2020. "Initial Impacts of Global Risk Mitigation Measures Taken During the Combatting of the COVID-19 Pandemic." *Safety Science*

128: art. 104773, 1–8. https://doi.org/10.1016/j.ssci.2020.104773

Buonanno, G., L. Morawska, and L. Stabile. 2020a. "Quantitative Assessment of the Risk of Airborne Transmission of SARS-CoV-2 Infection: Prospective and Retrospective Applications." *Environment International* 145: art. 106112, 1–10. https://doi.org/10.1016/j.envint.2020.106112

Buonanno, G., L. Stabile, and L. Morawska. 2020b. "Estimation of Airborne Viral Emission: Quanta Emission Rate of SARS-CoV-2 for Infection Risk Assessment." *Environment International* 141: art. 105794, 1–8. https://doi.org/10.1016/j.envint.2020.105794

Casagrande, D., and M. Piller. 2020. "Conflicting Effects of a Portable Ultra-Clean Airflow Unit on the Sterility of Operating Rooms: A Numerical Investigation." *Building and Environment* 171: art. 106643, 1–12. https://doi.org/10.1016/j.buildenv.2020.106643

Chen, Q. 1995. "Comparison of Different k-ε Models for Indoor air Flow Computations." *Numer. Heat Transf. Part B Fundam* 28: 353–369. https://doi.org/10.1080/10407799508928838.

Chen, F., S. C. M. Yu, and A. C. K. Lai. 2006. "Modeling Particle Distribution and Deposition in Indoor Environments with a new Drift-Flux Model." *Atmospheric Environment* 40: 357–367. https://doi.org/10.1016/j.atmosenv.2005.09.044.

Chung, I. P., and D. Dunn-Rankin. 1998. "Using Numerical Simulation to Predict Ventilation Efficiency in a Model Room." *Energy and Buildings* 28: 43–50. https://doi.org/10.1016/S0378-7788(97)00061-3.

Cirrincione, L., F. Plescia, C. Ledda, V. Rapisarda, D. Martorana, R. E. Moldovan, K. Theodoridou, and E. Cannizzaro. 2020. "COVID-19 Pandemic: Prevention and Protection Measures to be Adopted at the Workplace." *Sustainability* 12: 1–18. https://doi.org/10.3390/SU12093603.

Cole, E. C., and C. E. Cook. 1998. "Characterization of Infectious Aerosols in Health Care Facilities: An aid to Effective Engineering Controls and Preventive Strategies." *American Journal of Infection Control* 26: 453–464. https://doi.org/10.1016/S0196-6553(98)70046-X.

Dai, H., and B. Zhao. 2020. "Association of the Infection Probability of COVID-19 with Ventilation Rates in Confined Spaces." *Building Simulation* 13 (6): 1321–1327. https://doi.org/10.1007/s12273-020-0703-5.

D'angelo, D., A. Sinopoli, A. Napoletano, S. Gianola, G. Castellini, A. del Monaco, A. J. Fauci, et al. 2021. "Strategies to Exiting the COVID-19 Lockdown for Workplace and School: A Scoping Review." *Safety Science* 134: art. 105067, 1–8. https://doi.org/10.1016/j.ssci.2020.105067.

Di Gilio, A., J. Palmisani, M. Pulimeno, F. Cerino, M. Cacace, A. Miani, and G. de Gennaro. 2021. "CO2 Concentration Monitoring Inside Educational Buildings as a Strategic Tool to Reduce the Risk of Sars-CoV-2 Airborne Transmission." *Environmental Research* 202: art. 111560, 1–10. https://doi.org/10.1016/j.envres.2021.111560.

D'Orazio, M., G. Bernardini, and E. Quagliarini. 2021. "A Probabilistic Model to Evaluate the Effectiveness of Main Solutions to COVID-19 Spreading in University Buildings According to Proximity and Time-Based Consolidated Criteria." *Building Simulation* 14: 1795–1809. https://doi.org/10.1007/s12273-021-0770-2.

Elghobashi, S. 1994. "On Predicting Particle-Laden Turbulent Flows." *Applied Scientific Research* 52: 309–329. https://doi.org/10.1007/BF00936835.

Escombe, A. R., C. C. Oeser, R. H. Gilman, M. Navincopa, E. Ticona, W. Pan, C. Martínez, et al. 2007. "Natural Ventilation for the Prevention of Airborne Contagion." *PLoS Medicine* 4: 0309–0317. https://doi.org/10.1371/journal.pmed.0040068.

European Committee for Standardization. 2016. EN 12207 - Windows and Doors - Air Permeability - Classification.

Fang, Z., Z. Huang, X. Li, J. Zhang, W. Lv, L. Zhuang, X. Xu, and N. Huang. 2020. How Many Infections of COVID-19 There Will Be in the "Diamond Princess"-Predicted by a Virus Transmission Model based on the Simulation of Crowd Flow. arXiv:2002.10616v1.

Feng, G., Y. Zhang, and X. Lan. 2012. "Numerical Study of the Respiratory Aerosols Transportation in Ventilated Classroom." *Applied Mechanics and Materials* 204-208: 4298–4304. https://doi.org/10.4028/www.scientific.net/AMM.204-208.4298.

Fuoco, F. C., L. Stabile, G. Buonanno, C. V. Trassiera, A. Massimo, A. Russi, M. Mazaheri, L. Morawska, and A. Andrade. 2015. "Indoor Air Quality in Naturally Ventilated Italian Classrooms." *Atmosphere (Basel)* 6: 1652–1675. https://doi.org/10.3390/atmos6111652.

Gao, N., J. Niu, and L. Morawska. 2008. "Distribution of Respiratory Droplets in Enclosed Environments Under Different air Distribution Methods." *Building Simulation* 1: 326–335. https://doi.org/10.1007/s12273-008-8328-0.

Gao, X., J. Wei, H. Lei, P. Xu, B. J. Cowling, and Y. Li. 2016. "Building Ventilation as an Effective Disease Intervention Strategy in a Dense Indoor Contact Network in an Ideal City." *PLoS One* 11: 1–20. https://doi.org/10.1371/journal.pone.0162481.

Girardin, M., E. Bilgen, and P. Arbour. 1983. "Experimental Study of Velocity Fields in a Human Nasal Fossa by Laser Anemometry." *Annals of Otology, Rhinology & Laryngology* 92 (3): 231–236. https://doi.org/10.1177/000348948309200304.

Haug, N., L. Geyrhofer, A. Londei, E. Dervic, A. Desvars-Larrive, V. Loreto, B. Pinior, S. Thurner, and P. Klimek. 2020. "Ranking the Effectiveness of Worldwide COVID-19 Government Interventions." *Nature Human Behaviour* 4: 1303–1312. https://doi.org/10.1038/s41562-020-01009-0.

Hu, T., Y. Ji, F. Fei, M. Zhu, T. Jin, P. Xue, and N. Zhang. 2022. "Optimization of COVID-19 Prevention and Control with low Building Energy Consumption." *Building and Environment* 219: art. 109233, 1–11. https://doi.org/10.1016/j.buildenv.2022.109233.

Huang, L., S. Riyadi, I. K. A. P. Utama, M. Li, P. Sun, and G. Thomas. 2022. "COVID-19 Transmission Inside a Small Passenger Vessel: Risks and Mitigation." *Ocean Engineering* 255: art. 111486, 1–14. https://doi.org/10.1016/j.oceaneng.2022.111486.

Iddon, C., B. Jones, P. Sharpe, M. Cevik, and S. Fitzgerald. 2022. "A Population Framework for Predicting the Proportion of People Infected by the far-Field Airborne Transmission of SARS-CoV-2 Indoors." *Building and Environment* 221: art. 109309, 1–12. https://doi.org/10.1016/j.buildenv.2022.109309.

INFN. 2022. CovidStat INFN [WWW Document] (in Italian). Gruppo di Lavoro CovidStat INFN, Istituto Nazionale di Fisica Nucleare (National Institute for Nuclear Physics). URL https://covid19.infn.it (Last accessed: 2022/12/07).

ISTAT. 2022. Population and Households [WWW Document]. Istituto Nazionale di Statistica (Italian National Institute of Statistics). URL https://www.istat.it/en/population-and-households?data-and-indicators (Last accessed 2022/12/07).

Italian Parliament. 2005.. Lgs. D. 19 August 2005 No. 192. Implementation of the 2002/91/EC Directive on Energy Performance in Construction. Rome.

Italian Parliament. 2020. Law 22 May 2020, No. 35. Conversion into Law, with Amendments, of Decree-Law 25 March 2020, No. 19, Containing Urgent Measures for the Containment and Management of the Epidemiological Emergency from COVID-19.

Italian Parliament. 2021. Law 17 June 2021, No. 87. Conversion into Law, with Amendments, of Decree-Law 22 April 2021, No. 52, Containing Urgent Measures for the Gradual Resumption of Economic and Social Activities While Respecting the Need to Contain the Spread of the COVID-19 Epidemic.

Kampf, G., Y. Brüggemann, H. E. J. Kaba, J. Steinmann, S. Pfaender, S. Scheithauer, and E. Steinmann. 2020. "Potential Sources, Modes of Transmission and Effectiveness of Prevention Measures Against SARS-CoV-2." *Journal of Hospital Infection* 106: 678–697. https://doi.org/10.1016/j.jhin.2020.09.022.

Kuerten, J. G. M. 2016. "Point-Particle DNS and LES of Particle-Laden Turbulent Flow – A State-of-the-Art Review." *Flow, Turbulence and Combustion* 97: 689–713. https://doi.org/10.1007/s10494-016-9765-y.

Kundu, P. K., and I. M. Cohen. 2002. *Fluid Mechanics*. 2nd ed. San Diego, CA, USA: Academic Press.

Lai, A. C. K., and W. W. Nazaroff. 2000. "Modeling Indoor Particle Deposition from Turbulent Flow Onto Smooth Surfaces." *Journal of Aerosol Science* 31: 463–476. https://doi.org/10.1016/S0021-8502(99)00536-4.

Lee, J. H., M. Rounds, F. McGain, R. Schofield, G. Skidmore, I. Wadlow, K. Kevin, et al. 2022. "Effectiveness of Portable air Filtration on Reducing Indoor Aerosol Transmission: Preclinical Observational Trials." *Journal of Hospital Infection* 119: 163–169. https://doi.org/10.1016/j.jhin.2021.09.012.

Leung, N. H. L., D. K. W. Chu, E. Y. C. Shiu, K.-H. Chan, J. J. McDevitt, B. J. P. Hau, H.-L. Yen, et al. 2020. "Respiratory Virus Shedding in Exhaled Breath and Efficacy of Face Masks." *Nature Medicine* 26: 676–680. https://doi.org/10.1038/s41591-020-0843-2.

Li, A., and G. Ahmadi. 1992. "Dispersion and Deposition of Spherical Particles from Point Sources in a Turbulent Channel Flow." *Aerosol Science and Technology* 16: 209–226. https://doi.org/10.1080/02786829208959550.

Li, C., and H. Tang. 2022. "Comparison of COVID-19 Infection Risks Through Aerosol Transmission in Supermarkets and Small Shops." *Sustainable Cities and Society* 76: art. 103424, 1–11. https://doi.org/10.1016/j.scs.2021.103424.

Liu, X., J. Niu, M. Perino, and P. Heiselberg. 2008. "Numerical Simulation of Inter-Flat air Cross-Contamination Under the Condition of Single-Sided Natural Ventilation." *Journal of Building Performance Simulation* 1: 133–147. https://doi.org/10.1080/19401490802250462.

Lu, W., A. T. Howarth, N. Adam, and S. B. Riffati. 1996. "Modelling and Measurement of Airflow and Aerosol Particle Distribution in a Ventilated two-Zone Chamber." *Building and Environment* 31: 417–423. https://doi.org/10.1016/0360-1323(96)00019-4.

Meyerowitz, E. A., A. Richterman, R. T. Gandhi, and P. E. Sax. 2021. "Transmission of SARS-CoV-2: A Review of Viral, Host, and Environmental Factors." *Annals of Internal Medicine* 174: 69–79. https://doi.org/10.7326/M20-5008.

Ministry of Economic Development, Ministry of Environment and Land and Sea Protection, Ministry of Infrastructure and Transportation. 2015. M.D. 26 June 2015. Application of energy performance calculation methodologies and definition of minimum building requirements. Rome.

Mirzaie, M., E. Lakzian, A. Khan, M. E. Warkiani, O. Mahian, and G. Ahmadi. 2021. "COVID-19 Spread in a Classroom Equipped with Partition – A CFD Approach." *Journal of Hazardous Materials* 420: art. 126587, 1–18. https://doi.org/10.1016/j.jhazmat.2021.126587.

Mizumoto, K., and G. Chowell. 2020. "Transmission Potential of the Novel Coronavirus (COVID-19) Onboard the Diamond Princess Cruises Ship, 2020." *Infectious Disease Modelling* 5: 264–270. https://doi.org/10.1016/j.idm.2020.02.003.

Morawska, L., and J. Cao. 2020. "Airborne Transmission of SARS-CoV-2: The World Should Face the Reality." *Environment International* 139: art. 105730, 1–3. https://doi.org/10.1016/j.envint.2020.105730.

Morawska, L., and D. K. Milton. 2020. "It Is Time to Address Airborne Transmission of Coronavirus Disease 2019 (COVID-19)." *Clinical Infectious Diseases* 71: 2311–2313. https://doi.org/10.1093/cid/ciaa939.

Morawska, L., J. W. Tang, W. Bahnfleth, P. M. Bluyssen, A. Boerstra, G. Buonanno, J. Cao, et al. 2020. "How Can Airborne Transmission of COVID-19 Indoors be Minimised?" *Environment International* 142: 1–7. https://doi.org/10.1016/j.envint.2020.105832.

Naftali, S., R. C. Schroter, R. J. Shiner, and D. Elad. 1998. "Transport Phenomena in the Human Nasal Cavity: A Computational Model." *Annals of Biomedical Engineering* 26: 831–839. https://doi.org/10.1114/1.108.

Neeraj Mohan, V. P., and A. Pattamatta. 2015. "Implementation of two-Layer Realizable k-ϵ Turbulence Model Into OpenFOAM for the Simulation of Nuclear Reactor Cooling System.International ISHMT-ASTFE Heat and Mass Transfer Conference (IHMTC).Thiruvananthapuram, India. 17–20 December.

Nicas, M., W. W. Nazaroff, and A. Hubbard. 2005. "Toward Understanding the Risk of Secondary Airborne Infection: Emission of Respirable Pathogens." *Journal of Occupational and Environmental Hygiene* 2: 143–154. https://doi.org/10.1080/15459620590918466.

Noakes, C. J., C. B. Beggs, P. A. Sleigh, and K. G. Kerr. 2006. "Modelling the Transmission of Airborne Infections in Enclosed Spaces." *Epidemiology and Infection* 134: 1082–1091. https://doi.org/10.1017/S0950268806005875.

NPARC. 2022. Computational Fluid Dynamics (CFD) Verification and Validation Web Site of the NPARC Alliance – Section: Examining Spatial (Grid) Convergence [WWW Document]. URL https://www.grc.nasa.gov/www/wind/valid/tutorial/spatconv.html (Last accessed: 2022/12/02).

Pan, Y., D. Zhang, P. Yang, L. L. M. Poon, and Q. Wang. 2020. "Viral Load of SARS-CoV-2 in Clinical Samples." *The Lancet Infectious Diseases* 20: 411–412. https://doi.org/10.1016/S1473-3099(20)30113-4.

Peng, S., Q. Chen, and E. Liu. 2020. "The Role of Computational Fluid Dynamics Tools on Investigation of Pathogen Transmission: Prevention and Control." *Science of The Total Environment* 746: art. 142090, 1–23. https://doi.org/10.1016/j.scitotenv.2020.142090.

Pope, S. B. 2000. *Turbulent Flows*. Cambridge: Cambridge University Press.

Posner, J. D., C. R. Buchanan, and D. Dunn-Rankin. 2003. "Measurement and Prediction of Indoor air Flow in a Model Room." *Energy and Buildings* 35: 515–526. https://doi.org/10.1016/S0378-7788(02)00163-9.

Prather, K. A., C. C. Wang, and R. T. Schooley. 2020. "Reducing Transmission of SARS-CoV-2: Masks and Testing are Necessary to Combat Asymptomatic Spread in Aerosols and Droplets." *Science* 368: 1422–1424. https://doi.org/10.1126/science.abc6197.

Prem, K., Y. Liu, T. W. Russell, A. J. Kucharski, R. M. Eggo, N. Davies, S. Flasche, et al. 2020. "The Effect of Control Strategies to Reduce Social Mixing on Outcomes of the COVID-19 Epidemic in Wuhan, China: A Modelling Study." *The Lancet Public Health* 5: e261–e270. https://doi.org/10.1016/S2468-2667(20)30073-6.

Prentiss, M., A. Chu, and K. K. Berggren. 2022. "Finding the Infectious Dose for COVID-19 by Applying an Airborne-Transmission Model to Superspreader Events." *PLoS ONE* 17: art. e0265816, 1–23. https://doi.org/10.1371/journal.pone.0265816.

President of Italian Republic. 2013. D.R.P. 16 April 2013 No. 74. Regulation defining general criteria for operation, management, control, maintenance and inspection of systems for heating, cooling and DHW production in buildings, according to art. 4, subsection 1 a) and c), Lgs. D. 19 August.

Rencken, G. K., E. K. Rutherford, N. Ghanta, J. Kongoletos, and L. Glicksman. 2021. "Patterns of SARS-CoV-2 Aerosol Spread in Typical Classrooms." *Building and Environment* 204: art. 108167, 1–21. https://doi.org/10.1016/j.buildenv.2021.108167.

Riley, R. L. 2001. "How It Really Happened. What Nobody Needs to Know About Airborne Infection." *Am. J. Respir. Crit. Care Med* 163: 7–8. https://doi.org/10.1164/ajrccm.163.1.hh11-00.

Riley, E. C., G. Murphy, and R. L. Riley. 1978. "Airborne Spread of Measles in a Suburban Elementary School." *American Journal of Epidemiology* 107: 421–432. https://doi.org/10.1093/oxfordjournals.aje.a112560.

Roache, P. J. 1994. "Perspective: A Method for Uniform Reporting of Grid Refinement Studies." *Journal of Fluids Engineering* 116: 405–413. https://doi.org/10.1115/1.2910291.

Ronchi, E., and R. Lovreglio. 2020. "EXPOSED: An Occupant Exposure Model for Confined Spaces to Retrofit Crowd Models During a Pandemic." *Safety Science* 130: art. 104834, 1–8. https://doi.org/10.1016/j.ssci.2020.104834.

Rubinow, S. I., and J. B. Keller. 1961. "The Transverse Force on a Spinning Sphere Moving in a Viscous Fluid." *Journal of Fluid Mechanics* 11: 447–459. https://doi.org/10.1017/S0022112061000640.

Saari, A., T. Tissari, E. Valkama, and O. Seppänen. 2006. "The Effect of a Redesigned Floor Plan, Occupant Density and the Quality of Indoor Climate on the Cost of Space, Productivity and Sick Leave in an Office Building-A Case Study." *Building and Environment* 41: 1961–1972. https://doi.org/10.1016/j.buildenv.2005.07.012.

Saffman, P. G. 1965. "The Lift on a Small Sphere in a Slow Shear Flow." *Journal of Fluid Mechanics* 22: 385–400. https://doi.org/10.1017/S0022112065000824.

Schade, W., V. Reimer, M. Seipenbusch, and U. Willer. 2021. "Experimental Investigation of Aerosol and CO2 Dispersion for Evaluation of COVID-19 Infection Risk in a Concert Hall." *International Journal of Environmental Research and Public Health* 18 (6): art. 3037, 1–11. https://doi.org/10.3390/ijerph18063037.

Schiller, L. 1935. "A Drag Coefficient Correlation." *Zeit. Ver. Deutsch. Ing* 77: 318–320.

Secchi, S., A. Astolfi, G. Calosso, D. Casini, G. Cellai, F. Scamoni, C. Scrosati, and L. Shtrepi. 2017. "Effect of Outdoor Noise and Façade Sound Insulation on Indoor Acoustic Environment of Italian Schools." *Applied Acoustics* 126: 120–130. https://doi.org/10.1016/j.apacoust.2017.05.023.

Sharma, P., S. S. Bahga, and A. Gupta. 2023. "Modeling of Dispersion of Aerosolized Airborne Pathogens Exhaled in Indoor Spaces." *Physics of Fluids* 35: art. 047105, 1–16. https://doi.org/10.1063/5.0142869.

Shih, T.-H., W. W. Liou, A. Shabbir, Z. Yang, and J. Zhu. 1995. "A new k-ε Eddy Viscosity Model for High Reynolds Number Turbulent Flows." *Computers & Fluids* 24: 227–238. https://doi.org/10.1016/0045-7930(94)00032-T.

Sonkin, L. S. 1951. "The Role of Particle Size in Experimental air-Borne Infection." *American Journal of Epidemiology* 53: 337–354. https://doi.org/10.1093/oxfordjournals.aje.a119459.

Stabile, L., M. Dell'Isola, A. Frattolillo, A. Massimo, and A. Russi. 2016. "Effect of Natural Ventilation and Manual Airing on Indoor air Quality in Naturally Ventilated Italian Classrooms." *Building and Environment* 98: 180–189. https://doi.org/10.1016/j.buildenv.2016.01.009.

Szałański, P., W. Cepiński, and M. A. Sayegh. 2023. "Leakage in air Handling Units, the Effects on the Transmission of Airborne Infections." *Building and Environment* 233: art. 110074, 1–16. https://doi.org/10.1016/j.buildenv.2023.110074.

Sze To, G. N., and C. Y. H. Chao. 2010. "Review and Comparison Between the Wells-Riley and Dose-Response Approaches to Risk Assessment of Infectious Respiratory Diseases." *Indoor Air* 20: 2–16. https://doi.org/10.1111/j.1600-0668.2009.00621.x.

J.W. Tang, A.D. Nicolle, C.A. Klettner, J. Pantelic, L. Wang, A.B. Suhaimi, A.Y.L. Tan, et al. 2013. "Airflow Dynamics of Human Jets: Sneezing and Breathing - Potential Sources of Infectious Aerosols." *PLoS One* 8: 1–7. https://doi.org/10.1371/journal.pone.0059970.

van Doremalen, N., T. Bushmaker, D. H. Morris, M. G. Holbrook, A. Gamble, B. N. Williamson, A. Tamin, et al. 2020. "Aerosol and Surface Stability of SARS-CoV-2 as Compared with SARS-CoV-1. N." *New England Journal of Medicine* 382: 1564–1567. https://doi.org/10.1056/NEJMc2004973.

Vuorinen, V., M. Aarnio, M. Alava,V. Alopaeus, N. Atanasova, M. Auvinen, N. Balasubramanian, et al. 2020. "Modelling Aerosol Transport and Virus Exposure with Numerical Simulations in Relation to SARS-CoV-2 Transmission by Inhalation Indoors." *Safety Science* 130: art. 104866, 1–23. https://doi.org/10.1016/j.ssci.2020.104866.

Wang, J., and T.-T. Chow. 2015. "Influence of Human Movement on the Transport of Airborne Infectious Particles in Hospital." *Journal of Building Performance Simulation* 8: 205–215. https://doi.org/10.1080/19401493.2014.905636.

Wang, Z., E. R. Galea, A. Grandison, and J. Ewer. 2021. "Inflight Transmission of COVID-19 Based on Experimental Aerosol Dispersion Data." *Journal of Travel Medicine* 28: 1–7. https://doi.org/10.1093/jtm/taab023.

Wang, Z., E. R. Galea, A. Grandison, J. Ewer, and F. Jia. 2022. "A Coupled Computational Fluid Dynamics and Wells-Riley Model to Predict COVID-19 Infection Probability for Passengers on Long-Distance Trains." *Safety Science* 147: art. 105572, 1–18. https://doi.org/10.1016/j.ssci.2021.105572.

Watanabe, T., T. A. Bartrand, M. H. Weir, T. Omura, and C. N. Haas. 2010. "Development of a Dose-Response Model for SARS Coronavirus." *Risk Analysis* 30: 1129–1138. https://doi.org/10.1111/j.1539-6924.2010.01427.x.

Welsch, R., M. Wessels, C. Bernhard, S. Thönes, and C. von Castell. 2021. "Physical Distancing and the Perception of Interpersonal Distance in the COVID-19 Crisis." *Scientific Reports* 11: art. 11485, 1–9. https://doi.org/10.1038/s41598-021-90714-5.

Wolfshtein, M. 1969. "The Velocity and Temperature Distribution in one-Dimensional Flow with Turbulence Augmentation and Pressure Gradient." *International Journal of Heat and Mass Transfer* 12: 301–318. https://doi.org/10.1016/0017-9310(69)90012-X.

Zhang, R., G. Tu, and J. Ling. 2008. "Study on Biological Contaminant Control Strategies Under Different Ventilation Models in Hospital Operating Room." *Building and Environment* 43: 793–803. https://doi.org/10.1016/j.buildenv.2007.01.018.

Zhao, B., Y. Zhang, X. Li, X. Yang, and D. Huang. 2004. "Comparison of Indoor Aerosol Particle Concentration and Deposition in Different Ventilated Rooms by Numerical Method." *Building and Environment* 39: 1–8. https://doi.org/10.1016/j.buildenv.2003.08.002.

Appendices

1. Validation of the numerical model

The incompressible Navier-Stokes equations with Reynolds Averaged Navier-Stokes turbulence modelling are solved numerically with the commercial solver Simcenter STAR-CCM+®, version 2021.1.3 by Siemens Digital Industries Software.

For validation purposes, the experimental test by Chen, Yu, and Lai (2006) is reproduced by numerical simulation. A model room, as shown in Figure A1, is ventilated by a forced air-flow supplied from a vent opening in the upper part of a side wall, while an outlet vent is located in the lower part of the opposite wall. Both vents are square with dimensions 0.04 m × 0.04 m, with centres located at x = 0 m, y = 0.2 m, z = 0.36 m and x = 0.8 m, y = 0.2 m, z = 0.04 m, respectively. The size of the room is 0.8 m × 0.4 m × 0.4 m in terms of length (along x), width (along y) and height (along z), respectively. Hollow glass, silver coated spheres with a mean diameter of 10 µm are injected with a solid particle disperser. The density of the particles is 1.4×10^3 kg m^{-3}.

Chen, Yu, and Lai (2006) measure both the airflow velocity and the particle concentration with a phase Doppler anemometry (PDA) system. Olive oil droplets are used as tracers for the measurement of the fluid velocity components. The airflow mean velocity at the supply vent is 0.225 m/s.

The comparison between numerical and experimental results for the x-velocity component is illustrated in Figure A2, where data acquired along three evenly-spaced vertical sampling lines (see Figure A1) are considered and several turbulence models are compared. Among the considered turbulence models, the Reynolds Stress (RSM) and the standard k−ε turbulence models attain the best agreement with the experimental data. The standard and the Realizable k−ε models and the RSM model give rise to a relatively intense recirculation zone underneath the ceiling jet, which is not evident in the experimental data. Table A1 reports a quantitative comparison between numerical and experimental results in terms of the following root-mean-square-error metric:

$$\varepsilon_U = \sqrt{\frac{1}{N}\sum_{j=1}^{N}(U_{num,j} - U_{exp,j})^2} \tag{A1}$$

where, for given profile position, N is the number of available points, and $U_{num,j}$ [m/s] and $U_{exp,j}$ [m/s] are the numerical and experimental, respectively, values of horizontal velocity component.

In view of the obtained results, both the RSM and the k−ε turbulence models appear capable of reproducing the velocity profiles with a degree of accuracy that is deemed adequate for the purposes of the present investigation.

The steady-state concentration of the dispersed particles, scaled by the inlet concentration, is sampled along the aforementioned vertical sampling lines and results are shown in Figure A3. All considered models underestimate the particle concentration. The Realizable k−ε model provides better agreement with the experimental data in the region of the ceiling jet,

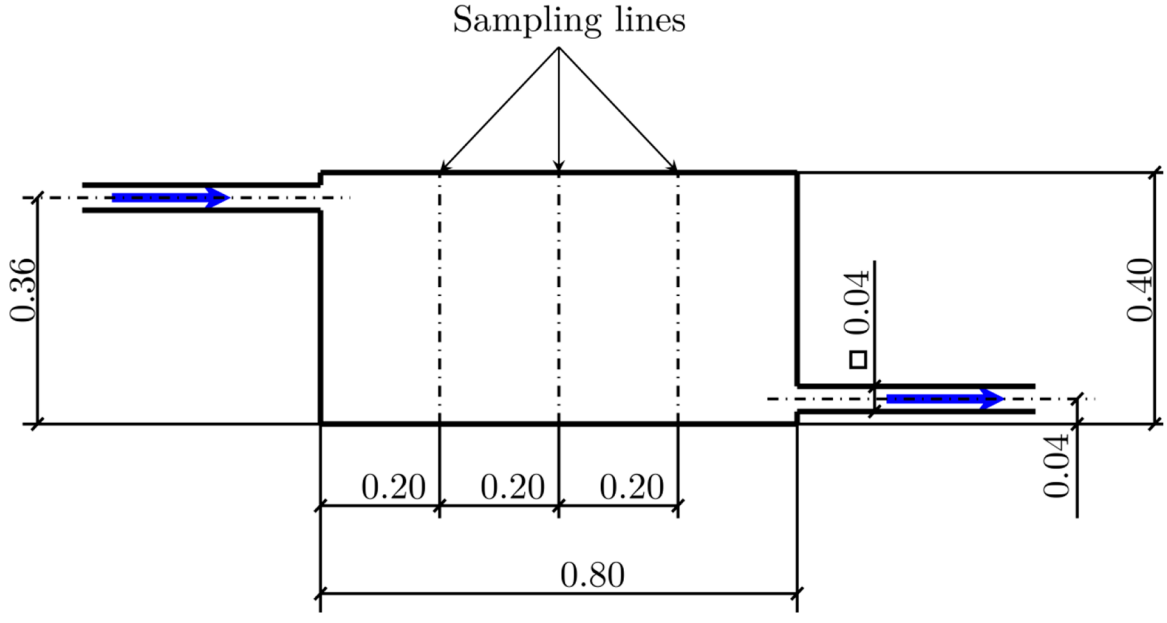

Figure A1. Sketch of the model room.

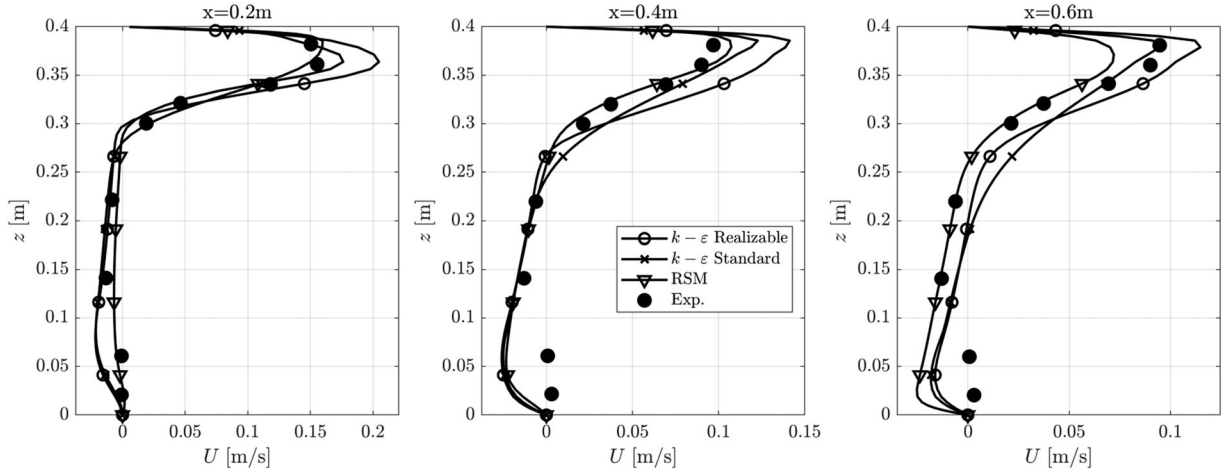

Figure A2. Comparison of experimental (Chen, Yu, and Lai 2006) and numerical x-component of velocity along the three considered sampling lines.

Table A1. Comparison between numerical and experimental results for horizontal velocity component, in terms of metric ε_U [m/s], for different turbulence models at the three considered profile positions.

Profile position x [m]	k-ε Realizable	k-ε Standard	RSM
0.2	0.022	0.0099	0.0096
0.4	0.027	0.016	0.011
0.6	0.016	0.013	0.017

Table A2. Comparison between numerical and experimental results for scaled particle concentration, in terms of metric ε_{C/C_i} [-], for different turbulence models at the three considered profile positions.

Profile position x [m]	k-ε Realizable	k-ε Standard	RSM
0.2	0.069	0.086	0.083
0.4	0.077	0.114	0.109
0.6	0.060	0.089	0.078

although the corresponding position is not accurately captured. Globally, the considered models reproduce the large-scale variation of the concentration along the sampling lines, though the details are missed. Table A2 reports a quantitative comparison between numerical and experimental results in terms of the root-mean-square-error metric ε_{C/C_i} [-], that is defined as ε_U (see (A.1)), but replacing the velocity component U with the scaled particle concentration C/C_i.

2. Turbulence modelling

The incompressible Navier-Stokes equations with Reynolds Averaged Navier-Stokes turbulence modelling are solved numerically with the commercial solver Simcenter STAR-CCM+®, version 2021.1.3 by Siemens Digital Industries Software.

The air is considered as a Newtonian ideal gas, and its weak density variations are mainly caused by the uneven temperature distribution throughout the classroom. Therefore, the Boussinesq approximation is used to represent the effect of the buoyancy forces (Kundu and Cohen 2002). The Realizable k $-$ ε turbulence model (RKE) provides the influence of the unresolved turbulent velocity fluctuations on the corresponding time-averaged quantities (Shih et al. 1995). The RKE model enforces certain mathematical constraints on the turbulent stresses: the turbulent normal stresses must be non-negative,

$$\overline{(u_t')^2} \geq 0 \tag{A2}$$

while the turbulent shear stresses must obey the Schwartz inequality,

$$\overline{u_i' \cdot u_j'} \leq \sqrt{\overline{(u_i')^2} \cdot \overline{(u_j')^2}} \tag{A3}$$

This goal is fulfilled by re-defining the dependence of the turbulent viscosity μ_t on the turbulent kinetic energy k and on its dissipation rate ε, while also providing some modifications to the model transport equation for ε (Pope 2000).

The 2-Layer near-wall treatment is applied (Neeraj Mohan and Pattamatta 2015). Accordingly, the flow domain is subdivided into a viscosity-affected region and into a fully turbulent region based on a threshold value for the wall-distance turbulent Reynolds number Re_d,

$$Re_d \equiv \frac{\sqrt{k} \cdot d}{\nu} \tag{A4}$$

where d denotes the distance from the nearest wall. In the fully-turbulent region, $Re_d > 200$, the RKE model provides k, ε and μ_t. For $Re_d \leq 200$ the turbulent dissipation rate is prescribed according to the wall-distance d (Wolfshtein 1969), while k is still determined by the RKE model. Further details on the RKE model with the 2-Layer near-wall treatment are available in Neeraj Mohan and Pattamatta (2015).

The calculation of the turbulent heat flux $\boldsymbol{q_t}$ relies on the gradient-diffusion hypothesis (Pope 2000), whose main assumption is that $\boldsymbol{q_t}$ is parallel to the mean temperature gradient and proportional to it via a turbulent thermal conductivity k_t, which, in turn, is related to the turbulent viscosity μ_t:

$$k_t = \frac{\mu_t \cdot c_p}{\sigma_t} \tag{A5}$$

where $\sigma_t = 0.9$ denotes the turbulent Prandtl number.

Table A3. Most relevant features of the considered computational meshes.

Mesh	N	PH [%]	δ [mm]	ϑ [°]	$< y^+ >$ [-]	max(y^+) [-]
1	1'554'356	86.87	5.86	36.81	34	325
2	2'994'130	90.00	4.67	35.36	27	319
3	5'824'743	91.97	3.57	35.57	24	256

3. Assessment of the sensitivity to the computational mesh

A set of three computational meshes is generated and numerical simulations of the airflow and particle distribution are carried out on each mesh. The calculated values of selected quantities are then compared among the three meshes to infer the corresponding order of convergence and an estimate of the uncertainty of grid convergence via the Grid Convergence Index (CGI) (Roache 1994). The considered meshes are generated via the snappyHexMesh utility of the open-source CFD package OpenFoam. The mesh generation algorithm progresses through three stages. In stage 1, the cells of a background hexahedral mesh are progressively split, resulting into a polyhedral mesh. In the optional second stage the mesh is morphed to better conform to the boundary of the computational domain. In a third optional stage cell layers are grown on wall boundaries. The aforementioned stages are governed via user-supplied parameters. As for this mesh-sensitivity study the mesh-generation governing parameters are kept fixed while the background mesh is progressively refined. At each refinement stage the number of computational cells grows by a factor of approximately 1.9. Table A3 reports the most relevant features of the considered computational meshes, namely: the number of computational cells N, the percentage PH of hexahedral cells, the minimum distance δ between the centroids of neighbor cells, the maximum skewness angle ϑ for interior cells, the surface-averaged ($< y^+ >$) and the maximum (max(y^+)) values of y^+ on the solid enclosure of the classroom.

The ventilation scenario 21 of the considered case study (see Table 5) is simulated to assess the uncertainty related to grid convergence. The quantities used in the present analysis to quantify the uncertainty in the airflow calculations are reported in Table A4 and correspond to mass-averaged values over the entire domain. For each quantity, the estimated order of convergence p, the GCI index for both the intermediate and the fine grid, and the relative difference between the solutions computed on the intermediate and fine meshes, ε_h, are calculated according to Roache (1994), except for the substitution of the 'factor of safety' 3.0 with the 'factor of safety' 1.25, as suggested by NPARC (2022) for cases where three meshes are used to estimate the order of convergence p.

In view of the obtained results, it was decided to use the intermediate mesh in the reported simulations of the case study.

4. Robustness of scenarios ranking

In section 3.5, ranking of different scenarios has been performed on the basis of the probability index $P_{Sbl}(t)$, as determined by

Table A4. Estimated order of convergence and GCI.

Quantity	Order of convergence	GCI for the intermediate-grid solution (%)	GCI for the fine-grid solution (%)	ε_h (%)
Mass-averaged turbulent kinetic energy	1.42	16.6	12.6	3.7
Mass-averaged kinetic energy	1.35	5.4	4.1	1.1
Mass-averaged temperature	1.51	1.1	0.8	−0.25

Table A5. Ranking matrix, with values in [%]. Exposure time: 5 h, with 10 min intense ventilation every hour.

Scen. ID	I	II	III	IV	V	VI
00	0.00	0.00	0.00	0.02	3.32	96.66
01	0.00	0.00	0.00	0.00	96.68	3.32
02	0.00	0.00	53.62	46.36	0.00	0.02
10	0.00	0.00	46.38	53.62	0.00	0.00
20	25.81	74.19	0.00	0.00	0.00	0.00
21	74.19	25.81	0.00	0.00	0.00	0.00

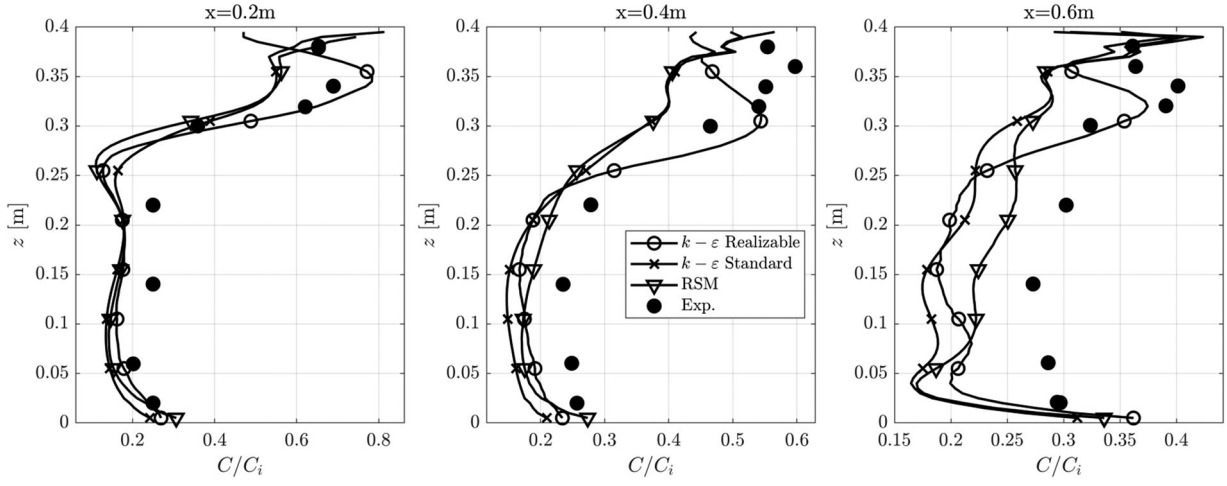

Figure A3. Comparison of experimental (Chen, Yu, and Lai 2006) and numerical scaled particle concentration along the three considered sampling lines.

using the assumed reference values of calculation parameters. However, as reported in section 3.1, calculation parameters are associated with an intrinsic level of uncertainty, and different values of model parameters may lead to different outcomes in terms of ranking of ventilation scenarios.

The scope of this Appendix is to investigate the robustness of the obtained ranking with respect to variations in the assumed values of calculation parameters. The analysis is carried out considering only variations in parameters c_v, c_i, p and v. All calculations are carried out assuming the same values of parameters for all occupants in the room, as done in the case study in section 3.

Specifically, the following discretizations have been used:

- c_v: uniformly discretized in logarithmic scale, with 41 values in the range 10^8–10^{11} RNA copies/mL of saliva;
- c_i: uniformly discretized in logarithmic scale, with 41 values in the range 10^{-2}–10^{-1} (RNA copies)$^{-1}$;
- p, v: uniformly discretized in linear scale, with 41 values in the range 0.5–1.25 m^3 h^{-1} and using $p = v$ (see (9)).

Accordingly, a total of $41^3 = 68921$ combinations of modified calculation parameters have been considered, and calculations were carried out considering the case of 5-hour exposure time (with intense ventilation for 10 min every hour, as in section 3.5). For each combination of parameters, each ventilation scenario has been given a ranking based on the obtained probability $P_{SbI}(t = 5h)$.

From the obtained data, it is possible to define a square $N_s \times N_s$ ranking matrix $\boldsymbol{R}$, where $N_s = 6$ is the number of ventilation scenarios, and the generic element R_{sr} corresponds to the fraction of considered combinations of parameters where the s-th scenario has been ranked in the r-th position.

Table A5 reports the obtained ranking matrix.

The results reported in Table A5 allow for a more robust comparison of the ventilation efficiency of the different considered scenarios.

The ventilation scenarios where PACs operate at the highest flow-rate (20 and 21) always reach the best ranking. Moreover, the ventilation scenario 02 ranks third in terms of P_{SbI}, whereas the scenario 10 ranks fourth. According to Table A5, the two scenarios have nearly the same fraction of combinations ranking either third or fourth, suggesting a similarity in terms of performance between the PACs activation at a low flow-rate and a condition of high permeability of the windows.

5. Example case of room with three occupants

The scope of the section is to clarify the application of the general probabilistic model (see section 2.3) to a case which is minimally simple, yet it contains the main essential features that can be found in more complex cases.

Therefore, a simplified notional case of a room with three occupants is considered. The occupants are numbered 1, 2 and 3. The details of their location in the room, as well as the geometry of the hypothetical room are irrelevant for the scope of the discussion herein.

For the considered 3-occupants example case, there are eight possible layouts, i.e. eight possible combinations of infected/not infected occupants at initial time, as reported in Table A6. For each layout, Table A6 reports the corresponding representative vector $\boldsymbol{k}$ (see (5)) and the corresponding probability of occurrence $P_{\boldsymbol{k}}$ (see (6)). The order used for the layouts is irrelevant to the final results. In this example, it has been decided to order the layouts on the basis of the number of SOIs in the room. Hence, layout #1 has no SOIs, layouts #2–#4 have exactly one SOI, layouts #5–#7 have exactly two SOIs, and, finally, layout #8 has exactly three SOIs.

It is assumed that relevant CFD and associated particle dispersion pre-calculations have been carried out, to provide the normalized concentrations $C'_{jn}(t)$ (see (8)). In this case, there are $3 \times 3 = 9$ normalized concentration functions $C'_{jn}(t)$ with $j, n = 1, 2, 3$. Correspondingly, there are nine doses $D_{jn}(t)$ with $j, n = 1, 2, 3$ (see (7)). For instance, the dose inhaled by the occupant $j = 1$ within an exposure time t due to the saliva droplets exhaled by the occupant $n = 3$ is:

$$D_{1,3}(t) = \int_0^t c_{v,3} \cdot C_{1,3}(\tau) \cdot p_1 d\tau = \int_0^t c_{v,3} \cdot C'_{1,3}(\tau) \cdot v_3 \cdot p_1 d\tau \tag{A6}$$

Doses $D_{jn}(t)$ can be properly superimposed to get the total dose inhaled by each SOI in each layout (see (10) and (11)).

For layout #1 (see Table A6), there are no SOIs and all occupants are SUIs. Therefore, according to expectation, and in line with (10) and (11), the inhaled dose is zero at each time instant for all the occupants, i.e.

$$\boldsymbol{k} = [0, 0, 0] \rightarrow \begin{cases} D_{1|\boldsymbol{k}}(t) = 0 \\ D_{2|\boldsymbol{k}}(t) = 0 \\ D_{3|\boldsymbol{k}}(t) = 0 \end{cases} \tag{A7}$$

The corresponding probabilities of infection for each SUI are also identically zero (see (12) and (13)), i.e.

$$\boldsymbol{k} = [0, 0, 0] \rightarrow \begin{cases} P_{SbI,1|\boldsymbol{k}}(t) = 0 \\ P_{SbI,2|\boldsymbol{k}}(t) = 0 \\ P_{SbI,3|\boldsymbol{k}}(t) = 0 \end{cases} \tag{A8}$$

For layouts #2-#4 (see Table A6), there is one SOIs and two SUIs. In this case, each SUI inhales the dose due to the saliva droplets exhaled by the unique SOI in the room. For instance, in case of layout #2, the only SOI is occupant 1, and the dose inhaled by the two SUIs (occupants 2 and 3) are (see (10) and (11)):

$$\boldsymbol{k} = [1, 0, 0] \rightarrow \begin{cases} D_{2|\boldsymbol{k}}(t) = D_{2,1}(t) \\ D_{3|\boldsymbol{k}}(t) = D_{3,1}(t) \end{cases} \tag{A9}$$

The infection probability for each occupant can be determined as follows (see (12) and (13))

$$\boldsymbol{k} = [1, 0, 0] \rightarrow \begin{cases} P_{SbI,1|\boldsymbol{k}}(t) = 0 \\ P_{SbI,2|\boldsymbol{k}}(t) = f_P(D_{2|\boldsymbol{k}}(t)) = 1 - e^{-c_{i,2} \cdot D_{2|\boldsymbol{k}}(t)} \\ P_{SbI,3|\boldsymbol{k}}(t) = f_P(D_{3|\boldsymbol{k}}(t)) = 1 - e^{-c_{i,3} \cdot D_{3|\boldsymbol{k}}(t)} \end{cases} \tag{A10}$$

where, first, the results have been reported in terms of general dose-response model (see (12)) and then in terms of the specific Wells-Riley exponential model (see (13)). Similar considerations apply to layouts #3 and #4.

For layouts #5–#7 (see Table A6), there are two SOIs and one SUIs. In this case, the unique SUI inhales the dose obtained by the superposition of contributions from the two SOIs in the room. For instance, in case of layout #5, the occupant 1 is a SUI, while occupants 2 and 3 are SOI. Accordingly, the dose inhaled by occupant 1 is (see (10) and (11))

$$\boldsymbol{k} = [0, 1, 1] \rightarrow D_{1|\boldsymbol{k}}(t) = D_{1,2}(t) + D_{1,3}(t) \tag{A11}$$

Table A6. Possible layouts and corresponding probabilities of occurrence for the 3-occupants example case. The symbol 'I' indicates SOIs, while the symbol '-' indicates a SUI.

Layout index	Occ.1	Occ.2	Occ.3	$\boldsymbol{k}$	$P_{\boldsymbol{k}}$
#1	–	–	–	[0,0,0]	$(1-P_{I,1})\cdot(1-P_{I,2})\cdot(1-P_{I,3})$
#2	I	–	–	[1,0,0]	$P_{I,1}\cdot(1-P_{I,2})\cdot(1-P_{I,3})$
#3	–	I	–	[0,1,0]	$(1-P_{I,1})\cdot P_{I,2}\cdot(1-P_{I,3})$
#4	–	–	I	[0,0,1]	$(1-P_{I,1})\cdot(1-P_{I,2})\cdot P_{I,3}$
#5	–	I	I	[0,1,1]	$(1-P_{I,1})\cdot P_{I,2}\cdot P_{I,3}$
#6	I	–	I	[1,0,1]	$P_{I,1}\cdot(1-P_{I,2})\cdot P_{I,3}$
#7	I	I	–	[1,1,0]	$P_{I,1}\cdot P_{I,2}\cdot(1-P_{I,3})$
#8	I	I	I	[1,1,1]	$P_{I,1}\cdot P_{I,2}\cdot P_{I,3}$

The infection probability for each occupant can be determined as follows (see (12) and (13))

$$\boldsymbol{k}=[0,1,1]\rightarrow\begin{cases}P_{SbI,1|\boldsymbol{k}}(t)=f_P(D_{1|\boldsymbol{k}}(t))=1-e^{-c_{i,1}\cdot D_{1|\boldsymbol{k}}(t)}\\P_{SbI,2|\boldsymbol{k}}(t)=0\\P_{SbI,3|\boldsymbol{k}}(t)=0\end{cases}\tag{A12}$$

where, also in this case, first, the result has been reported in terms of general dose-response model (see (12)) and then in terms of the specific Wells-Riley exponential model (see (13)).

Similar considerations apply to layouts #6 and #7.

In case of layout #8 (see Table A6) all occupants are SOI. Therefore, the determination of inhaled doses is not relevant, and the probability of getting infected for each occupant is zero by definition (see (12) and (13)), i.e.

$$\boldsymbol{k}=[1,1,1]\rightarrow\begin{cases}P_{SbI,1|\boldsymbol{k}}(t)=0\\P_{SbI,2|\boldsymbol{k}}(t)=0\\P_{SbI,3|\boldsymbol{k}}(t)=0\end{cases}\tag{A13}$$

It is noted that the knowledge of $P_{SbI,1|\boldsymbol{k}}(t)$, $P_{SbI,2|\boldsymbol{k}}(t)$ and $P_{SbI,3|\boldsymbol{k}}(t)$ for each given layout $\boldsymbol{k}$ allows also a direct determination of the corresponding conditional expected (mean) number of infection transmissions considering an exposure time t, $\bar{N}_{SbI|\boldsymbol{k}}(t)$, as follows (see (24) and (25))

$$\bar{N}_{SbI|\boldsymbol{k}}(t)=P_{SbI,1|\boldsymbol{k}}(t)+P_{SbI,2|\boldsymbol{k}}(t)+P_{SbI,3|\boldsymbol{k}}(t)\tag{A14}$$

The conditional probabilities $P_{SnI|\boldsymbol{k}}(t)$ that no SUI gets infected for each given layout $\boldsymbol{k}$ considering an exposure time t (see (20)), and the corresponding conditional probabilities $P_{SbI|\boldsymbol{k}}(t)$ (see Table 1) that at least one SUI gets infected for each given layout $\boldsymbol{k}$ considering an exposure time t, can be determined as shown in Table A7. It is noted that, in reporting results in Table A7, the outcomes from the general formulation (20) have already been simplified accounting for cases with probabilities $P_{SbI,j|\boldsymbol{k}}(t)=0$.

The marginal probability $P_{SbI}(t)$ that least one SUI gets infected considering an exposure time t can be obtained according to (22), using probabilities $P_{\boldsymbol{k}}$ (see Table A6) and $P_{SbI|\boldsymbol{k}}$ (see Table A7), as follows

$$\begin{aligned}P_{SbI}(t)&=\sum_{\boldsymbol{k}}P_{SbI|\boldsymbol{k}}(t)\cdot P_{\boldsymbol{k}}\\&=P_{SbI|\boldsymbol{k}=[0,0,0]}(t)\cdot P_{\boldsymbol{k}=[0,0,0]}+P_{SbI|\boldsymbol{k}=[1,0,0]}(t)\cdot P_{\boldsymbol{k}=[1,0,0]}\\&\quad+P_{SbI|\boldsymbol{k}=[0,1,0]}(t)\cdot P_{\boldsymbol{k}=[0,1,0]}+P_{SbI|\boldsymbol{k}=[0,0,1]}(t)\cdot P_{\boldsymbol{k}=[0,0,1]}\\&\quad+P_{SbI|\boldsymbol{k}=[0,1,1]}(t)\cdot P_{\boldsymbol{k}=[0,1,1]}+P_{SbI|\boldsymbol{k}=[1,0,1]}(t)\cdot P_{\boldsymbol{k}=[1,0,1]}\\&\quad+P_{SbI|\boldsymbol{k}=[1,1,0]}(t)\cdot P_{\boldsymbol{k}=[1,1,0]}+P_{SbI|\boldsymbol{k}=[1,1,1]}(t)\cdot P_{\boldsymbol{k}=[1,1,1]}\\&=P_{SbI|\boldsymbol{k}=[1,0,0]}(t)\cdot P_{\boldsymbol{k}=[1,0,0]}+P_{SbI|\boldsymbol{k}=[0,1,0]}(t)\cdot P_{\boldsymbol{k}=[0,1,0]}\\&\quad+P_{SbI|\boldsymbol{k}=[0,0,1]}(t)\cdot P_{\boldsymbol{k}=[0,0,1]}+P_{SbI|\boldsymbol{k}=[0,1,1]}(t)\cdot P_{\boldsymbol{k}=[0,1,1]}\\&\quad+P_{SbI|\boldsymbol{k}=[1,0,1]}(t)\cdot P_{\boldsymbol{k}=[1,0,1]}+P_{SbI|\boldsymbol{k}=[1,1,0]}(t)\cdot P_{\boldsymbol{k}=[1,1,0]}\end{aligned}\tag{A15}$$

where use has been made of the fact that $P_{SbI|\boldsymbol{k}=[0,0,0]}(t)=0$ and $P_{SbI|\boldsymbol{k}=[1,1,1]}(t)=0$ (see Table A7).

In addition, the limit of $P_{SbI}(t)$ as the exposure time tends to infinity, $P_{SbI,lim}$, can be determined according to (23) as

$$\begin{cases}P_{SbI,lim}=1-(P_{\boldsymbol{k}=[0,0,0]}+P_{\boldsymbol{k}=[1,1,1]})\\with\\P_{\boldsymbol{k}=[0,0,0]}=(1-P_{I,1})\cdot(1-P_{I,2})\cdot(1-P_{I,3})\\P_{\boldsymbol{k}=[1,1,1]}=P_{I,1}\cdot P_{I,2}\cdot P_{I,3}\end{cases}\tag{A16}$$

Finally, the marginal expected (mean) number of transmissions considering an exposure time t, $\bar{N}_{SbI}(t)$, can be determined as follows (see (26))

$$\begin{aligned}\bar{N}_{SbI}(t)&=\sum_{\boldsymbol{k}}\bar{N}_{SbI|\boldsymbol{k}}(t)\cdot P_{\boldsymbol{k}}\\&=\bar{N}_{SbI|\boldsymbol{k}=[0,0,0]}(t)\cdot P_{\boldsymbol{k}=[0,0,0]}+\bar{N}_{SbI|\boldsymbol{k}=[1,0,0]}(t)\cdot P_{\boldsymbol{k}=[1,0,0]}\\&\quad+\bar{N}_{SbI|\boldsymbol{k}=[0,1,0]}(t)\cdot P_{\boldsymbol{k}=[0,1,0]}+\bar{N}_{SbI|\boldsymbol{k}=[0,0,1]}(t)\cdot P_{\boldsymbol{k}=[0,0,1]}\\&\quad+\bar{N}_{SbI|\boldsymbol{k}=[0,1,1]}(t)\cdot P_{\boldsymbol{k}=[0,1,1]}+\bar{N}_{SbI|\boldsymbol{k}=[1,0,1]}(t)\cdot P_{\boldsymbol{k}=[1,0,1]}\\&\quad+\bar{N}_{SbI|\boldsymbol{k}=[1,1,0]}(t)\cdot P_{\boldsymbol{k}=[1,1,0]}\\&\quad+\bar{N}_{SbI|\boldsymbol{k}=[1,1,1]}(t)\cdot P_{\boldsymbol{k}=[1,1,1]}=\\&=\bar{N}_{SbI|\boldsymbol{k}=[1,0,0]}(t)\cdot P_{\boldsymbol{k}=[1,0,0]}\\&\quad+\bar{N}_{SbI|\boldsymbol{k}=[0,1,0]}(t)\cdot P_{\boldsymbol{k}=[0,1,0]}+\bar{N}_{SbI|\boldsymbol{k}=[0,0,1]}(t)\cdot P_{\boldsymbol{k}=[0,0,1]}\\&\quad+\bar{N}_{SbI|\boldsymbol{k}=[0,1,1]}(t)\cdot P_{\boldsymbol{k}=[0,1,1]}+\bar{N}_{SbI|\boldsymbol{k}=[1,0,1]}(t)\cdot P_{\boldsymbol{k}=[1,0,1]}\\&\quad+\bar{N}_{SbI|\boldsymbol{k}=[1,1,0]}(t)\cdot P_{\boldsymbol{k}=[1,1,0]}\end{aligned}\tag{A17}$$

where use has been made of the fact that $\bar{N}_{SbI|\boldsymbol{k}=[0,0,0]}(t)=0$ and $\bar{N}_{SbI|\boldsymbol{k}=[1,1,1]}(t)=0$ (see (A8), (A13) and (A14)).

Table A7. Probabilities $P_{SnI|\boldsymbol{k}}(t)$ and $P_{SbI|\boldsymbol{k}}(t)$ for all possible layouts for the 3-occupants example case.

Layout index	$\boldsymbol{k}$	$P_{SnI|\boldsymbol{k}}(t)$	$P_{SbI|\boldsymbol{k}}(t)$
#1	[0,0,0]	1	0
#2	[1,0,0]	$(1-P_{SbI,2|\boldsymbol{k}}(t))\cdot(1-P_{SbI,3|\boldsymbol{k}}(t))$	$1-(1-P_{SbI,2|\boldsymbol{k}}(t))\cdot(1-P_{SbI,3|\boldsymbol{k}}(t))$
#3	[0,1,0]	$(1-P_{SbI,1|\boldsymbol{k}}(t))\cdot(1-P_{SbI,3|\boldsymbol{k}}(t))$	$1-(1-P_{SbI,1|\boldsymbol{k}}(t))\cdot(1-P_{SbI,3|\boldsymbol{k}}(t))$
#4	[0,0,1]	$(1-P_{SbI,1|\boldsymbol{k}}(t))\cdot(1-P_{SbI,2|\boldsymbol{k}}(t))$	$1-(1-P_{SbI,1|\boldsymbol{k}}(t))\cdot(1-P_{SbI,2|\boldsymbol{k}}(t))$
#5	[0,1,1]	$1-P_{SbI,1|\boldsymbol{k}}(t)$	$P_{SbI,1|\boldsymbol{k}}(t)$
#6	[1,0,1]	$1-P_{SbI,2|\boldsymbol{k}}(t)$	$P_{SbI,2|\boldsymbol{k}}(t)$
#7	[1,1,0]	$1-P_{SbI,3|\boldsymbol{k}}(t)$	$P_{SbI,3|\boldsymbol{k}}(t)$
#8	[1,1,1]	1	0